Department of Information and Communications Engineering

Multi-Antenna Ambient Backscatter Communications: Performance Optimization and Analysis

Xiyu Wang

Aalto University

DOCTORAL THESES

Aalto University publication series
DOCTORAL THESES 117/2023

Multi-Antenna Ambient Backscatter Communications: Performance Optimization and Analysis

Xiyu Wang

A doctoral thesis completed for the degree of Doctor of Science (Technology) to be defended, with the permission of the Aalto University School of Electrical Engineering, at a public examination held at the lecture hall AS1, TUAS building of the school on 08 September 2023 at 12:00.

Aalto University
School of Electrical Engineering
Department of Information and Communications Engineering
Communications Engineering

Supervising professor
Professor Riku Jäntti, Aalto University, Finland

Thesis advisor
Doctor Hüseyin Yiğitler, Aalto University, Finland

Preliminary examiners
Professor Donatella Darsena, University of Napoli Parthenope, Italy
Professor Markku Juntti, University of Oulu, Finland

Opponent
Professor Aggelos Bletsas, Technical University of Crete, Greece

Aalto University publication series
DOCTORAL THESES 117/2023

ISBN 978-952-64-1365-5 (printed)
ISBN 978-952-64-1366-2 (pdf)
ISSN 1799-4934 (printed)
ISSN 1799-4942 (pdf)
http://urn.fi/URN:ISBN:978-952-64-1366-2

Unigrafia Oy
Helsinki 2023

Finland

NORDIC SWAN ECOLABEL
Printed matter
4041-0619

Aalto University

Abstract

Aalto University, P.O. Box 11000, FI-00076 Aalto www.aalto.fi

Author
Xiyu Wang

Name of the doctoral thesis
Multi-Antenna Ambient Backscatter Communications: Performance Optimization and Analysis

Publisher School of Electrical Engineering

Unit Department of Information and Communications Engineering

Series Aalto University publication series DOCTORAL THESES 117/2023

Field of research Communications Engineering and Networking Technology

Manuscript submitted 6 April 2023 **Date of the defence** 8 September 2023

Permission for public defence granted (date) 19 June 2023 **Language** English

☐ **Monograph** ☒ **Article thesis** ☐ **Essay thesis**

Abstract

Amid the evolution of Internet-of-things (IoT), connecting the ever-increased number of devices requires sustainable solutions. Ambient backscatter communications (AmBC) emerges as a promising enabler because of its ultra-low power consumption and maximized spectrum efficiency. Wider deployment of AmBC is confronted with the need to increase the communication range and achievable data rate of a backscatter device (BD). These two system performance indicators are limited by the poor bit error rate (BER) performance of demodulating the BD signal due to its extremely low signal-to-noise ratio (SNR). In this thesis, AmBC receiver design and BD signaling matrix design are investigated to improve the AmBC system performance. Their implementation details are discussed to improve their practicality and generality. The results suggest that the proposed designs minimize BER compared to the state-of-the-art works, and thus foster a diversity of use cases.

The research in the thesis exploits multiple antennas to improve the SNR of the BD signal. A machine learning (ML)-assisted coherent receiver that obtains an SNR gain is proposed. The ML classification is used to estimate and compensate for the phase offset caused by the excess path length of the backscatter path channel compared to the direct path channel. In contrast, the proposed optimum receiver considers the composite channel of the two paths. As the phase offset is included in the composite channel, the non-coherent optimum receiver achieves the same BER performance as the coherent receiver. The derived receivers generalize to different AmBC deployments regardless of the types of BD modulation and ambient signals, and thus need not be tailored to specific system setups. Their performance analyses both suggest that BD placement close to the ambient source or AmBC receiver but away from the line segment between them yields a better BER performance. Furthermore, optimizing the reflection coefficients on a multi-antenna BD, termed a BD signaling matrix, maximizes backscatter signal strength. This is a particularly attractive solution in scenarios with multiple ambient sources.

The practicality of the presented designs is elaborated in depth and evaluated through experimentation. Methods for estimating the parameters of the AmBC receivers and the BD signaling matrix are proposed. Solutions are provided for mitigating the dynamic range issue of analog-to-digital converters when the receivers are implemented in the digital domain. The proposed multi-antenna AmBC receivers are verified to outperform the receivers in the literature through measurements from a prototyped AmBC system. A processing method is proposed to guarantee a successful implementation. Therefore, the thesis is composed of both theoretical derivation and practical demonstration of the designs that improve AmBC system performance.

Keywords Ambient backscatter communications, receiver design, performance analysis, reflection coefficients, multi-antennas, RF measurement

ISBN (printed) 978-952-64-1365-5 **ISBN (pdf)** 978-952-64-1366-2

ISSN (printed) 1799-4934 **ISSN (pdf)** 1799-4942

Location of publisher Helsinki **Location of printing** Helsinki **Year** 2023

Pages 173 **urn** http://urn.fi/URN:ISBN:978-952-64-1366-2

Preface

This thesis signals that my journey as a doctoral student at Aalto University has eventually come to an end. At this point, I would like to express my sincere gratitude to many incredible people who offered me help, guidance, and support throughout my doctoral study.

First and foremost, I feel extremely fortunate that I was able to join the strong group led by my supervisor Prof. Riku Jäntti, who is a role model with wisdom, enthusiasm, and professionalism in doing research. Thanks, Riku, for the guidance, the right amount of flexibility for students to do research, and for always being responsive when I needed help. I thank my advisor Dr. Hüseyin Yiğitler, a tenacious, high-capability, and articulate researcher who has provided me with valuable and insightful comments and feedback. All those times that you sat beside me helping me with paper-writing and technical problems (sometimes "fighting") are painful (only a bit) yet very stimulating and have greatly benefited my research development. Thank you both for your time and patience.

I would like to thank Ruifeng Duan who let me feel more welcome and helped me quickly integrate into the working environment after I had just arrived. Thank you for providing me with a smooth start on my doctoral study. I would also thank my other colleagues and collaborators: Bingqing Zhao, Boxuan Xie, Estifanos Menta, Jingyi Liao, Kalle Ruttik, Lauri Mela, Muhammad Sheikh, Nicolas Malm, Norshahida Saba, Viktor Nässi, and many others who were always willing to share their expertise and offer help. In addition, the chatting time that we had in the coffee room made my study fun and colorful.

I sincerely express my gratitude to my pre-examiners, Prof. Donatella Darsena and Prof. Markku Juntti for the useful comments and remarks. I would like to thank Prof. Aggelos Bletsas for accepting the invitation to act as my opponent of the defense.

I would like to dedicate this thesis to my family and my friends. Thanks, Mom and Dad, your unconditional love and support are precious in helping me achieve this milestone. And thank you, all my lovely friends from different periods of my life and die Südmenschen, for spicing up my journey with numerous joys. Finally, Marcel, no words can fully express my gratitude for you. All the wonderful moments and encouragements that we shared during these years are my support to reach the goal.

Espoo, July 10, 2023,

Xiyu Wang

Contents

List of Publications

This thesis consists of an overview and of the following publications which are referred to in the text by their Roman numerals.

I Ruifeng Duan, Xiyu Wang, Hüseyin Yiğitler, Muhammad Sheikh, Riku Jäntti, and Zhu Han. Ambient Backscatter Communication for Future Ultra-Low-Power Machine Type Communications: Challenges, Solutions, Opportunities, and Future Research Trends. *IEEE Communications Magazine*, vol. 58, no. 2, pp. 42-47, February 2020.

II Xiyu Wang, Ruifeng Duan, Hüseyin Yiğitler, Estifanos Yohannes Menta, and Riku Jäntti. Machine Learning-Assisted Detection for BPSK-Modulated Ambient Backscatter Communication Systems. In *IEEE Global Communications Conference (GLOBECOM)*, pp. 1-6, Hawaii, USA, 2019.

III Xiyu Wang, Hüseyin Yiğitler, Ruifeng Duan, Estifanos Yohannes Menta, and Riku Jäntti. Coherent Multiantenna Receiver for BPSK-Modulated Ambient Backscatter Tags. *IEEE Internet of Things Journal*, vol. 9, no. 2, pp. 1197-1211, January 2022.

IV Xiyu Wang, Hüseyin Yiğitler, and Riku Jäntti. A Simplified Multi-Antenna Receiver for General Binary-Modulated Ambient Backscatter Signal. In *IEEE Global Communications Conference (GLOBECOM)*, pp. 1-6, Madrid, Spain, 2021.

V Hüseyin Yiğitler, Xiyu Wang, and Riku Jäntti. Optimum Multi-antenna Ambient Backscatter Receiver for Binary-Modulated Tag Signals. *IEEE Transactions on Wireless Communications*, vol. 22, no. 2, pp. 808-823, February 2023.

VI Xiyu Wang, Hüseyin Yiğitler, and Riku Jäntti. Gaining from Multiple Ambient Sources: Signaling Matrix for Multi-Antenna Backscatter

Devices. *IEEE Wireless Communications Letters*, vol. 12, no. 3, pp. 491-495, March 2023.

VII Xiyu Wang, Hüseyin Yiğitler, Bing-Qing Zhao, Jingyi Liao, Norshaida Saba, Nicolas Malm, and Riku Jäntti. Implementation of Low-cost Multi-antenna AmBC Receivers. In *IEEE Vehicular Technology Conference Spring (VTC-Spring)*, pp. 1-6, Florence, Italy 2023.

Author's Contribution

Publication I: "Ambient Backscatter Communication for Future Ultra-Low-Power Machine Type Communications: Challenges, Solutions, Opportunities, and Future Research Trends"

The author had the main responsibity in literauture review and the writing of the sections entitled 'Direct Path Interference' and 'Receiver Design'.

Publication II: "Machine Learning-Assisted Detection for BPSK-Modulated Ambient Backscatter Communication Systems"

The author proposed the method and wrote the paper. The second and the fourth author assisted in providing the simulation resutls. The other authors reviewed the paper.

Publication III: "Coherent Multiantenna Receiver for BPSK-Modulated Ambient Backscatter Tags"

The author completed the work under the supervision of Prof. Riku Jäntti and Dr. Hüseyin Yiğitler. The other authors reviewed the work.

Publication IV: "A Simplified Multi-Antenna Receiver for General Binary-Modulated Ambient Backscatter Signal"

The author completed the work under the supervision of Prof. Riku Jäntti and Dr. Hüseyin Yiğitler.

Publication V: "Optimum Multiantenna Ambient Backscatter Receiver for Binary-Modulated Tag Signals"

Together with Dr. Hüseyin Yiğitler, the author developed the work, derived the receiver structures and analyzed their performance in Section III, and proposed the beamformer estimation method in Section IV. Other discussions on practical implementation were done by Dr. Hüseyin Yiğitler. The paper was written by the Dr. Hüseyin Yiğitler and the author. The work was supervised by Prof. Riku Jäntti.

Publication VI: "Gaining from Multiple Ambient Sources: Signaling Matrix for Multi-Antenna Backscatter Devices"

The author completed the work under the supervision of Prof. Riku Jäntti and Dr. Hüseyin Yiğitler.

Publication VII: "Implementation of Low-cost Multi-antenna AmBC Receivers"

The author designed the setup, carried out the measurement, analyzed the data and wrote the paper. The second author participated in discussing the processing method. The thrid and fourth author participated in carrying out the measurement. The fifth and sixth helped in preparing the receiver antenna array. The work was completed under the supervision of Prof. Riku Jäntti.

Abbreviations

3GPP	The 3rd Generation Partnership Project
ADC	Analog-to-digital converter
AIoT	Ambient Internet of things
AmBC	Ambient backscatter communications
ASK	Amplitude shift keying
BC	Backscatter communications
BD	Backscatter device
BER	Bit error rate
BPSK	Binary phase shift keying
COTS	Commercial off-the-shelf
DPI	Direct path interference
DVB-T	Digital video broadcasting - terrestrial
FSK	Frequency shift keying
i.i.d.	independent and identical distributed
IoT	Internet of things
I/Q	In-phase/quadrature
kNN	k-nearest neighbors
LDR	Linear discriminant analysis
LoRa	Long range
LR	Logistic regression
LTE	Long-term evolution
MAP	Maximum-a-posteriori

MIMO	Multiple input and multiple output
ML	Machine learning
MTC	Machine-type communications
OFDM	Orthogonal frequency-division multiplexing
OOK	On off keying
PCA	Principle component analysis
PDF	Probability density function
PSK	Phase shift keying
QPSK	Quadrature phase shift keying
QAM	Quadrature amplitude modulation
RF	Radio frequency
RFID	Radio frequency identification
RX	Receiver
SC	Selective combining
SIC	Successive interference cancellation
SDR	Software defined radio
SINR	Signal-to-interference-plus-noise ratio
SNR	Signal-to-noise ratio
SVM	Support vector machine
TX	Transmitter in an ambient system
ZF	Zero forcing

Symbols

$(\cdot)^H$	Conjugate-transpose operation
$(\cdot)^*$	Conjugate operation
$\lvert \cdot \rvert$	Absolute value
$\lVert \cdot \rVert$	Euclidean norm
$\lVert \cdot \rVert_\infty$	Infinity norm
$\lVert \cdot \rVert_F$	Frobenius norm
$\lVert \cdot \rVert_2$	L2-norm
$[\cdot]_j$	The j-th column of a matrix or the j-th element of a vector
$[\cdot]_{i,j}$	The i,j-th element of a matrix
$\boldsymbol{B}(x_i)$	Beamforming matrix when BD transmits x_i
$\boldsymbol{c}$	Component of $\boldsymbol{h}_b$ channel that is orthogonal to $\boldsymbol{h}_d$
$\mathbb{C}$	Complex space
$\mathcal{CN}(\boldsymbol{a}, \boldsymbol{A})$	Circularly symmetric complex Gaussian distribution with mean $\boldsymbol{a}$ and covariance matrix $\boldsymbol{A}$
d_0	Distance between TX and RX reference antenna
d_1	Distance between BD and RX reference antenna
d_2	Distance between TX and BD
$\mathrm{E}\{\cdot\}$	Expectation
$f(\cdot)$	Probability density function
f_c	Carrier frequency
$\boldsymbol{g}_i$	Composite channel vector when BD transmits x_i
$\boldsymbol{G}(x)$	Inverse of variance matrix of $\boldsymbol{y}$ when BD transmits x_i
$\boldsymbol{h}_d$	Normalized direct path channel vector

$\boldsymbol{h}_b$	Backscatter path channel vector normalized with respect to direct path channel
$\mathcal{H}_i$	Hypothesis i: x_i is transmitted from BD
$\boldsymbol{I}_n$	The $n \times n$ identity matrix and n may be omitted for simplicity
$\mathrm{Im}\{\cdot\}$	Imaginary part of a complex number
K	Oversampling rate
L	Length of preamble sequence
N_t	Number of antennas of ambient source
N_r	Number of antennas of AmBC receiver
N_b	Number of antennas of BD
$\boldsymbol{p}$	Position of BD
$\boldsymbol{p}_t$	Position of TX
$\boldsymbol{p}_{r,n_r}$	Position of the n_r-th RX antenna
$\Pr(\cdot)$	Probability
P_s	Averaged transmit power at TX
$\mathrm{Q}(\cdot)$	Q-function
$\boldsymbol{r}$	Residual signal of $\boldsymbol{y}$ after projecting into the null space of $\boldsymbol{h}_d$
$\boldsymbol{R}_{\boldsymbol{y}\|x}$	Conditional auto-correlation matrix of $\boldsymbol{y}$ conditioned on x
$\mathrm{Re}\{\cdot\}$	Real part of a complex number
$\boldsymbol{s}$	Ambient signal
V	Decision threshold
x	Signal transmitted from a single-antenna BD
$\boldsymbol{X}$	BD signaling matrix
$\boldsymbol{y}$	Temporal received sample on multi-antenna receiver
z	Test statistic of a receiver
Z_A	Antenna impedance
Z_L	Load impedance
α	Power loss on BD modulator circuit implementation
γ	Received SNR of ambient signal per RX antenna
γ_e	Effective SNR of backscatter signal

Γ	Reflection coefficient of BD modulator
η_2	Projection of $\boldsymbol{h}_b$ on $\boldsymbol{c}$
κ	Angular variation between $\boldsymbol{g}_0$ and $\boldsymbol{g}_1$
λ	Wavelength
μ_ℓ	The ℓ-th eigenvalue of a matrix
ρ_0	Fading loss of the direct path channel
ρ_1	Fading loss of the backscatter path channel
σ_s^2	Variance of the Gaussian-distributed ambient signal
$\boldsymbol{\Sigma}_{\boldsymbol{y}\|x}$	Conditional covariance matrix of $\boldsymbol{y}$ given x
ϕ	Phase offset caused by excess path length of backscatter path
$\boldsymbol{\omega}$	Additive white Gaussian noise at RX

1. Introduction

The roll-out of IoT technologies continues, aiming to provide an extremely wide range of applications including wireless sensing [1], tracking [2], assisting mobile communications [3] and many others. Advanced by sensor miniaturization, wireless communications and ubiquitous computing, IoT foresees a plethora of devices accessing the Internet. The total number of IoT devices is forecast to reach 34.7 billion in 2028 [4]. Hence, over the following decades, we may truly experience a world of connected buildings, furniture and agriculture.

As an integral part of IoT ecosystem, machine type communications (MTC) technologies provide an operational framework for different applications and services [5]. MTC manifests in wireless communications with a large number of sensors, actuators and other physical devices without the need for human intervention. The ongoing fifth generation (5G) and the future sixth generation (6G) wireless networks are natively designed to satisfy the MTC requirement of massive connections [6]. Using MTC in implementing the IoT paradigm is, however, restricted by four main factors: i) the applicability limited by the battery life of devices (Even though the longevity of a battery can be up to years, battery charging, replacement and maintenance further require resource); ii) the number of devices that can be deployed in an application which is constraint by the cost of each device; iii) the carbon footprint of an ever-increasing number of devices violating the Net Zero goal; iv) the spectrum availability limited by the congestion of the communication medium. Therefore, low-cost energy-efficient solutions are crucial for pervasive connectivity.

The urge for sustainable solutions has driven the 3rd Generation Partnership Project (3GPP) to introduce the concept of ambient IoT (AIoT) [7]. AIoT circumvents the replacement and recharge of batteries by considering battery-less devices. These battery-less devices resort to energy harvesting

techniques for their operations. However, power harvested from natural miniature sources, for example, thermal, solar and photovoltaic sources, is typically very low. The ultimate source of AIoT is ambient radio frequency (RF) signals transmitted in ambient systems[1]. Hence, compared to existing IoT technologies, such as narrowband-IoT and LTE-MTC, AIoT is promising to provide orders-of-magnitude lower complexity and power consumption.

The harvested power is often in the range of few microwatts [8] while the required power of active transceivers is in the order of milliwatts. As the amount of harvested power is not sufficient for active transceivers, backscatter communications (BC) comes to the fore. The idea of backscattering dates back to 1945 where a reader uses signal reflected from an aircraft to differentiate "friend" from "foe" [9]. In a typical BC system nowadays (e.g., radio frequency identification (RFID) system), a backscatter device (BD) (e.g., RFID tag) communicates to a nearby receiver (e.g., RFID reader) through modulating the incident signal [10]. The BD information is modulated by changing the reflection of the impinging signal, which requires no active RF components to generate radio waves. Thus, its power consumption is affordable using available energy harvesting techniques. Together with the low manufacturing cost of BDs, the benefits make BC an attractive MTC application scenario. However, the illuminating signal in a BC system usually comes from a carrier emitter that is dedicated for a BD. This dedicated power infrastructure, such as RFID reader, requires high power and occupies bandwidth to illuminate nearby BDs.

To further actualize the AIoT concept, the seminal work [11] proposed the novel ambient backscatter communications (AmBC) system. AmBC utilizes the RF signal permeating in the air to enable BD communications as well as to power BDs. Since AmBC systems share spectrum with ambient systems, AmBC technology maximizes spectrum utilization. As such, AmBC provides a complete solution for the four limitations stated above, and thus is expected to advance the evolution of MTC for next generation communications. It opens up various new use cases and enriches existing ones. For example, the use cases of AmBC are: i) pervasive sensing using a deployment of multiple passive sensors which greatly reduces the carbon footprint compared to conventional sensing systems with multiple

[1]Ambient systems denote the wireless communication systems existing in the air which generates RF signal serving its dedicated users. Detailed description is given in Chapter 2.

active transmitter-receiver pairs; ii) automatic asset tracking systems which are free from manual barcode scans [12]; iii) healthcare applications with in-vivo smart devices enabled by battery-less and small form factor BDs [13].

In this thesis, the AmBC system is the focal point, challenges related to the popularizing of AmBC are identified and solutions are investigated.

1.1 Motivation and Scope

The ultra-low-power, spectrum-efficient and low-cost AmBC enables IoT with massive connections and Net Zero greenhouse gas emissions. AmBC systems have the potential to be deployed for various purposes as pointed out in the previous section. Different deployment scenarios and purposes exert different requirements of communication range and/or achievable data rate of the BD signal on AmBC systems [14]. Thus, a wider range of use cases is contingent on communication range and/or data rate of the BD signal being improved. These two performance indicators are directly determined by AmBC receiver performance. Consequently, improving the AmBC receiver performance is of significance in opening up use-case possibilities.

Enhancing the receiver performance is challenging in AmBC systems because the performance is strongly limited by the low effective signal-to-noise ratio (SNR) of the target BD signal. An AmBC system exploiting ambient RF signals and using battery-free devices leaves a heavy burden on AmBC receivers. Often, there is a lack of cooperation between AmBC systems and ambient systems. Consequently, AmBC receivers have little information about ambient RF signals. The rapidly varying and unknown ambient RF signal has a similar effect of a fast fading channel towards BD signals. Second, an AmBC receiver receives the target signal together with a direct path signal that is transmitted from an ambient transmitter to the AmBC receiver. The direct path signal, denoted as *direct path interference* (DPI), is significantly stronger than the target BD signal [15], [16]. These two properties particularly diminish the effective SNR of the BD signal[2]. Therefore, AmBC receivers need to be carefully investigated to obtain

[2]The effective SNR of the BD signal denotes the ratio of the BD signal to the noise where DPI is not taken in account. In an AmBC system, effective SNR can be deduced from the SNR of the ambient signal and the power difference from the two paths.

acceptable performance.

Recently, the increasingly popular multiple-input and multiple-output (MIMO) technique has been integrated into AmBC systems [17], [18]. Using multiple antennas on AmBC receivers can mitigate DPI without the need for assistance from ambient system or complex channel information. This is realized by exploiting the spatial difference between the direct path signal and the backscatter path signal [19]. Deploying multiple antennas on BDs has also been considered to improve system performance through devising transmission schemes. It is able to provide diversity gains [20] and/or coding gains [21]. In addition, multiple antennas provide array gain which increases the effective SNR of the backscatter signal. Given these factors, using multiple antennas in AmBC systems is a practically advantageous method for improving receiver performance, which is considered in this thesis.

The objective of this thesis is to provide a comprehensive view of enhancing the receiver performance of BD signals in AmBC systems. In particular, bit error rate (BER) is selected as the performance evaluation criterion. The thesis seeks general solutions from the perspectives of both AmBC receivers and BD reflection coefficients. The research in the thesis theoretically derives AmBC receiver structures and BD reflection coefficients based on the criterion of minimizing probability of error of demodulating BD signals, which yields the optimum design [22]. Correspondingly, the second objective of this thesis is to improve the practicality of the designs by providing implications regarding implementations and carrying out experimentations.

The scope of this thesis focuses on the AmBC system with a single BD and its AmBC receiver. Although AmBC systems with multiple BDs feature more use cases, they are not considered in the following chapters. The considered AmBC system is generic where AmBC receivers can have some information about ambient systems, but does not know the specific signal transmitted by these ambient sources. An energy harvester is a necessary module inside a BD, but this thesis assumes that BDs have harvested enough energy for operations. Finally, even though the synchronization between a BD and its receiver is important, its strategy is not covered but perfect synchronization is assumed.

1.2 Contributions

The summarized publications in this thesis are related to improving the BER performance of AmBC systems. This thesis contributes to the research field in improving AmBC system performance so as to foster a diverse range of AmBC-enabled IoT use cases. This is made possible as several contributions enumerated below:

1. A machine learning (ML)-assisted coherent receiver for the binary phase shift keying (BPSK)-modulated BD signal is derived. A challenge relating to an unknown phase shift caused by the excess backscatter path length is identified. The solution of realizing phase-coherent operation is a simple ML classification algorithm. The receiver requires no prior information on ambient signal or on channels, and it obtains an SNR gain provided by the BPSK modulation and the phase-coherent operation.

2. Two optimum receivers for a general binary-modulated BD signal when the ambient signal is Gaussian-distributed and when the ambient signal is deterministic-unknown, i.e., there is no prior information available, are derived. The two optimum receivers are equivalent under certain conditions, which generalizes the optimum receiver in [23] by discussing that Gaussian ambient signal assumption is not required for most practical scenarios.

3. Theoretical probabilities of error of the coherent receiver and the two optimum receivers are derived. By analyzing these probabilities, key parameters affecting the performance are identified. The parameters lead to a unified deployment suggestion that good receiver performance is obtained when a BD is close to either the ambient source or AmBC receiver, but not in the line segment connecting the ambient source and the AmBC receiver.

4. It is shown that the optimum receivers are non-coherent but achieve the same performance as the coherent receiver. In the research of this thesis, the reason is that the optimum receivers explore the composite channel, in which the unknown phase offset of the backscatter path is included. As such, the optimum receivers have no phase-ambiguity.

5. Implementation solutions of the receivers that mitigates the dynamic range issue of an analog-to-digital converter (ADC) are given. AmBC

systems requires a high dynamic range when the receivers are implemented in the digital domain. A hybrid implementation is proposed which has the same performance as that of the fully-digital implementation. Another solution to overcome the dynamic range issue is a simplified receiver which can be implemented fully in the analog domain. Although the simplified receiver yields performance degradation, it is a cost-efficient solution because it saves half of the required front-ends.

6. It is shown when there are multiple ambient sources, using multiple antennas on a BD is necessary to make effective use of these ambient sources. The reflection coefficients on multi-antenna BDs, referred to as the BD signaling matrix, are optimized based on the criterion of minimizing the probability of error. The optimum BD signaling matrices enlarge the coverage of BDs compared to the commonly-used identity BD signaling matrix.

7. The proposed multi-antenna AmBC receivers together with several receivers presented in [19] are implemented through laboratory-scale measurements. For a successful implementation, a signal processing method is proposed to combat the disruption caused by the environment and the unstable commercial off-the-shelf (COTS) hardware components. Results show that the signal processing method is effective, and among the receivers, the proposed optimum receivers outperform the others.

1.3 Structure of the Thesis

The overall structure of the thesis consists of an introductory part of the seven publications that are appended to the second part of the thesis. The remainder of the introductory part is organized as follows.

Chapter 2 starts by introducing the AmBC systems followed by the signal model. The chapter points out the key components of the AmBC systems and summarizes the main challenges of implementing such systems.

Chapter 3 presents the designs proposed in the publications for improving the BER performance of the AmBC system. Specifically, a coherent receiver is summarized from Publication II, Publication III, and an optimum receiver is summarized from Publication V which is a non-coherent receiver. Thereafter, the BER performance is enhanced from the perspec-

tive of optimizing the BD reflection coefficients. The BD with multiple antennas introduced in Publication VI helps improve the BER performance, especially in the multiple ambient sources co-existence scenario.

In Chapter 4, challenges regarding practical implementation are discussed including estimating parameters for the receivers and the BD reflection coefficients, and the dynamic range issue. Two solutions for the dynamic range issue are proposed in Publication IV and Publication V. An AmBC system with a single-antenna BD and a low-cost AmBC receiver under a wideband ambient system is implemented. The receivers presented in Publication V, Publication IV, and existing literature are evaluated using the measurement data. The degradation in performance of the direct implementation caused by the wideband effect is identified and corresponding signal processing is proposed in Publication VII. Finally, the conclusions are drawn in Chapter 5.

2. Ambient Backscatter Communications

This chapter presents an overview of AmBC systems. Different deployments of AmBC systems are depicted first, followed by the description of BD modulator basics. The AmBC system model considered throughout the thesis is then presented. Finally, the reasons that hamper the BER performance of AmBC systems are described and available solutions in the literature are reviewed.

2.1 Overview

Backscatter denotes a type of communications where a device transmits its signal not by generating an RF signal, but by changing an RF signal that impinges on its antenna. The changed signal is re-radiated and is received by another device which recovers the signal. A typical backscatter type of communication system consists of a BD, a transmitter (TX) and a receiver (RX). As illustrated in Figure 2.1, such a system generally has the mono-static configuration, shown in (a) and (b), and the bi-static configuration, shown in (c) and (d), depending on whether the TX and RX are co-located or dis-located.

In a traditional BC system, the TX is often a carrier emitter that generates an RF carrier for the BD to modulate its signal on, and the co-located RX demodulates the signal reflected from the BD. AmBC differs from BC in the way that AmBC leverages RF signals already existing in the air, such as Bluetooth low energy [24]–[26], long range (LoRa) [27], [28], WiFi [25], [29], [30], digital video broadcasting - terrestrial (DVB-T) [11], frequency modulation (FM) radio [31] and long term evolution (LTE) signals [32], [33]. One important feature of AmBC systems is that an ambient system can be non-cooperative and completely unaware of the AmBC systems that make use of its signal. As such, AmBC systems can use either a joint RX for both

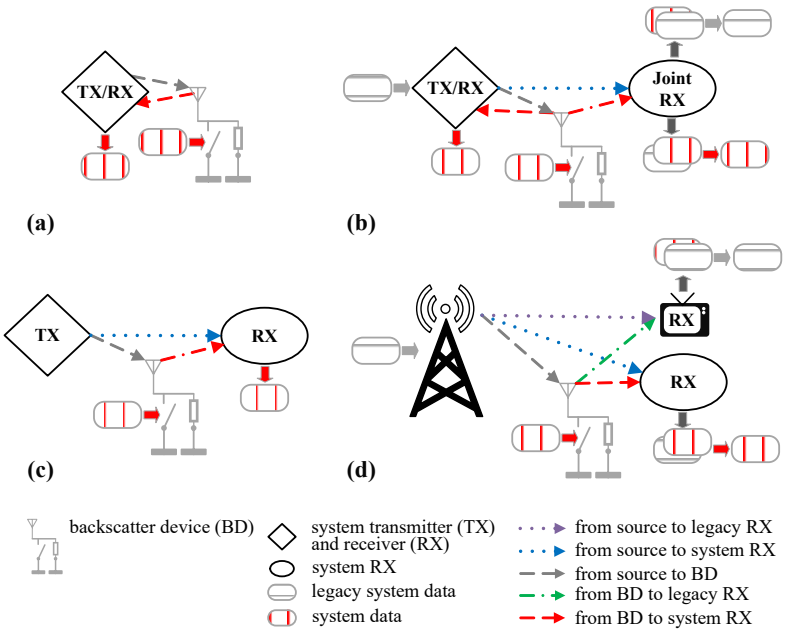

Figure 2.1. Backscattering and AmBC configurations: (a) mono-static BC; (b) mono-static AmBC and AmBC with a joint receiver; (c) bi-static BC; (d) AmBC with ambient and legacy receivers.

legacy and AmBC systems or a separate AmBC RX, shown in Figure 2.1 (b) and (d), respectively.

To compare the bi-static with the mono-static configuration, one can compare the link budget from the TX to the RX and that from the TX to the Joint RX in Figure 2.1 (b). The results show that mono-static has a lower link budget when the BD is more than a certain distance away from the TX [16][1]. The gap enlarges as the distance between the TX and the BD increases. This is because, in this case, the BD moves closer to the joint RX in bi-static configurations, whereas the BD signal in mono-static scenario suffers from round-trip path loss [34]. Hence, bi-static can obtain the benefit of a stronger BD signal strength by strategically deploying the BD close to either the TX or the RX. This gives a higher deployment flexibility without adding a higher manufacturing cost [35]. In this scenario, one RX can be used to serve multiple BDs illuminated by multiple carrier emitters. Moreover, the bi-static configuration further provides the possibility of device-to-device (D2D) communications by enabling transmissions within two BDs [36]. Provided with the above advantages, the bi-static configuration is preferable and thus, is considered in this work.

Passive BDs require energy for information processing and/or modula-

[1]The distance is a function of the carrier frequency.

tion operations. Without requiring a power-hungry RF signal generation block, power consumption of the backscattering devices is in the order of microwatts [37]. The ultra-low-power nature makes the state-of-the-art energy harvesting techniques feasible to provide energy for BDs. Compared to energy sources such as thermal and solar, ambient RF signal gives a higher stability as RF signals are ubiquitous and available regardless of the time [38]. The amount of energy that can be harvested from ambient RF signals is highly dependent on the RF signal conditions, the distance between the source and the BD, the harvesting duration as well as the harvesting efficiency [39], [40]. For instance, up to 60 microwatts can be supplied to a device from a DVB-T signal when a 960-kilowatts-powered TV tower is located 4.1 km away from it [8]. On the other hand, the amount of energy needed by BDs depends on transmission data rates and transmission time [41], [42]. In the passive WiFi prototype [43], 1 megabit-per-second and 11 megabit-per-second transmission consume 14.5 and 59.2 microwatts, respectively. The harvesting time of indoor devices is longer than that of outdoor devices using cellular networks due to the wall penetration loss [44]. In order to shorten the harvesting time, one can use hybrid sources. Nevertheless, since the scope of the thesis is the receiver performance for BD signals, it is assumed that BDs have harvested enough energy to support their operations.

2.2 Backscatter Device Modulator

The BD structure involves many modules including energy harvester, wake-up radio, modulator, and controller unit [29]. Since this thesis focuses on the performance of AmBC receivers, BD modulators and signals transmitted by BDs are of concern. In what follows, we first introduce the basics of a modulator for a single-antenna BD and then, extend it to a modulator for a multi-antenna BD.

2.2.1 Backscatter Basics

Modulation

A BD modulates its signal by changing an incoming RF signal. Depending on the modulation type, the frequency, amplitude, phase or a combination of phase and amplitude of an incoming signal can be changed. These correspond to frequency shift keying (FSK), amplitude shift keying (ASK), phase

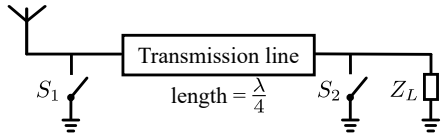

Figure 2.2. An illustration of a three-state BD modulator.

shift keying (PSK), and quadrature amplitude modulation (QAM), respectively. The resultant change is represented by the ratio of the reflected signal and the incoming signal. It is termed as the reflection coefficient, denoted by Γ. The core idea of changing the reflection coefficient is impedance mismatching [45], [46]. On a BD, this is realized by connecting the antenna directly to a load. Let Z_A be the complex antenna impedance, and Z_L be the load impedance. The complex reflection coefficient is given by [47]

$$\Gamma = \frac{Z_L - Z_A^*}{Z_L + Z_A}. \tag{2.1}$$

By altering the load impedance, the reflection coefficient is changed accordingly [48], [49].

A BD modulator realizing three states modulation, i.e., '0', '-1', and '+1', is shown in Figure 2.2. It consists of two single-pole switches S_1 and S_2 and a load with impedance Z_L that is equal to the conjugate of the antenna impedance. When the two switches S_1 and S_2 are open, the load impedance is matched with the antenna impedance. In this case, the signal is dissipated on the load and no signal is reflected back. This corresponds to the state of '0'. When one of the switches is closed, the load impedance $Z_L = 0$ so that the signal is reflected back. In addition, the length of $\lambda/4$ transmission line renders the equivalent antenna impedance to have a $\pi/2$ phase difference. Thus, these two states correspond to the reflection coefficient of '-1' and '+1', respectively.

The presented BD modulator is evidently able to perform the widely-adopted on-off keying (OOK) modulation [11], [31], [50], [51] and the binary phase shift keying (BPSK) modulation [29], [52]–[54]. Such a BD modulator can also perform frequency modulation by toggling between '0' and '1' states at a certain frequency. This toggling frequency denotes a key of the FSK modulation. The frequency modulation is to use the square wave for approximating a sine wave, which has been applied in BC and AmBC systems such as [32], [55], [56].

When performing ASK and PSK, the signal backscattered by a BD and the signal transmitted by a TX interfere with each other at the receiver, making it difficult to demodulate the BD signal especially if the signal from

the TX has a much higher signal strength. The interference can be filtered out by using FSK which shifts the spectrum of BD signals. However, FSK induces unwanted interference to other frequency bands [31]. For improving the efficiency of spectrum usage, this thesis focuses on non-frequency shift modulations.

Higher-order BD modulation can be realized by additional loads in a BD modulator, or by controlling a transistor with different voltage levels [57], [58]. Using higher-order modulation schemes increases BD data rate [54], [58], [59], which leads to a lower power consumption for transmission. However, a higher-order-modulated signal requires a complex receiver with a high-resolution demodulator especially in a low SNR region. Therefore, without loss of generality, binary modulations are considered for simplicity.

Non-frequency shift modulations allow mapping a BD modulation state directly to a reflection coefficient. Throughout the thesis, let $x = \Gamma$ denote the signal transmitted by a BD. BD signal is binary-modulated, that is, $x \in \{x_0, x_1\}$. The prior probability of a BD signal is $\Pr(x)$ and $\Pr(x_0) = 1 - \Pr(x_1)$. Without loss of generality, we assume the BD signal has an equal probability, i.e., $\Pr(x_0) = 0.5$.

Other backscatter device properties

An AmBC system coexists with an ambient system, and thus can be reckoned as a spectrum sharing system of the ambient system. The coexistence increases the achievable rate of an ambient system under the condition that the ambient system can track the channel variations caused by BD transmissions and take the backscatter path signal as a multipath component [60], [61]. This happens when a BD symbol is much longer than a symbol of the ambient system[2]. On the other hand, if a BD symbol duration is short such that ambient systems cannot track the channel variation, the backscatter path signal appears as interference. However, this rarely happens due to the passive property of BDs. Therefore, the existence of AmBC systems can be exploited to improve the performance of ambient systems.

In practice, BD modulator circuit implementation induces a power loss [15], [16]. This modulator loss may arise from mismatches of antenna impedance, transmission line characteristic impedance and/or impedance of a dissipating load, and a non-zero impedance of the switches when they are in the 'on' state. In practice, the power loss can be measured from the absolute

[2]This forms the foundation of the emerging reconfigurable intelligent surfaces (RIS) technology [62].

square of the S_{11} parameter of a vector network analyzer which indicates the ratio of output power and input power at the BD antenna port. The power loss decreases the power of the received backscatter signal and, in turn, affects the AmBC system performance. Therefore, in the following mathematical representation, the power loss is included and is denoted as α.

From antenna theory [63], the existence of a BD antenna in the propagation environment per se alters the channel between the TX and RX. This is known as the *structural mode* of BD antenna. This mode is load-independent and is due to the interaction between the incident field and the antenna structure [45]. The other part, which is controlled by the BD load impedance, is referred to as the *antenna mode*. A load selection rule for improving the tag efficiency is studied in [64]. For a passive BD performing OOK, for example, the mismatch load can be selected according to the structural mode in order to increase the backscatter signal power. This requires an estimate of the structural mode of the BD antenna and a careful BD circuitry design. This work considers a general binary modulation on BDs. As such, signals resulting from the antenna mode are of interest. The structural mode merely adds an additional multipath component to the channel between the TX and RX. It is included in the direct path channel, but has no effect on the BD signal demodulation. Therefore, the mathematical representation derived in this thesis is general and covers the impact of structural mode.

2.2.2 Multi-Antenna Backscatter Device

Configuring multiple antennas on passive BDs has been considered to improve the receiver performance [50], [65]. Let us consider a generic BD with N_b antennas. In this case, the BD signal, denoted by matrix $\boldsymbol{X} \in \mathbb{C}^{N_b \times N_b}$, is termed as the *BD signaling matrix*. The elements of a BD signaling matrix represent the reflection coefficient seen by BD antennas. There are three forms of BD signaling matrix defined depending on the physical implementation of the BD modulation circuitry. They are *identity signaling matrix*, *diagonal signaling matrix*, and *full signaling matrix* [20]. The identity signaling matrix and diagonal signaling matrix take a simpler form where no signal is transferred between the antenna elements. The reflection coefficients on BD antennas are represented by the diagonal elements of the signaling matrix. Their difference lies in whether the reflection coefficients on different antenna elements are the same. On the

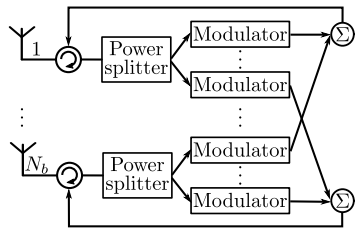

Figure 2.3. A realization of a multi-antenna BD modulator.

other hand, a full signaling matrix stands for a BD modulator that requires a signal transfer among different antenna elements. This signal transfer is represented by an off-diagonal element of the matrix. It is to be noted that unlike an active antenna array that needs synchronization between multiple local oscillators, a passive BD antenna array does not need local oscillators and hence, signals across different antennas are inherently synchronized.

An implementation of a multi-antenna BD modulator that is able to realize full signaling matrix modulation is shown in Figure 2.3. The incident signal on one BD antenna is split into N_b branches, each of which goes through a modulator. These N_b branches of the modulated signal then contribute individually to the signals that are backscattered from N_b BD antennas. In regard to the modulators for the identity or diagonal signaling matrix, for a single BD antenna, the power splitter and the $N_b - 1$ branches are omitted.

For a multi-antenna BD, a binary modulation implies that $\boldsymbol{X} \in \{\boldsymbol{X}_0, \boldsymbol{X}_1\}$. Furthermore, signaling matrices are subject to a power constraint because BDs have no active RF amplifiers. The power constraint reads as

$$\|[\boldsymbol{X}]_j\|^2 \leq 1, j = 1, \cdots, N_b, \tag{2.2}$$

where $[\cdot]_j$ denotes the j-th column vector of a matrix and $\|\cdot\|$ represents the Euclidean norm. The constraint implies that a signal will not be amplified after passing through N_b branches of modulators.

2.3 System Model

In this thesis, bi-static AmBC systems are considered due to their potentially extended communication range and higher deployment flexibility, as stated in Section 2.1. A typical bi-static AmBC system is shown in Figure 2.4. There is a single-antenna ambient source TX serving the user equipment of an ambient (legacy) system. A BD modulates its own signal

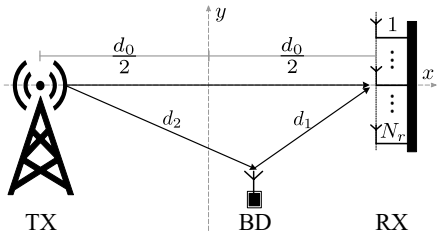

Figure 2.4. A bi-static AmBC system model. An ambient source (TX) and a multi-antenna AmBC receiver (RX) are placed on the horizontal axis of a Cartesian reference frame, and the mid-point of the line segment connecting the TX antenna and the RX reference antenna is set as the reference frame origin.

on the impinging ambient signal from the TX and re-radiates it from the antenna. A single-antenna BD is considered first and a multi-antenna BD is defined in Section 3.4. An AmBC receiver (RX) is equipped with a uniform linear array that has N_r antennas and half-wavelength separation between two adjacent elements. The RX receives a composite signal coming from two paths. One path is not affected by the BD modulator, termed as the *direct path signal*, including the signal directly from the ambient source as well as scattered signals caused by the structural mode of the BD antenna. The other path is modulated by the BD and is referred to as the *backscatter path signal*. The AmBC RX aims to demodulate the BD signal from this composite signal.

2.3.1 Channel Model

Throughout the thesis, we consider that the wireless channels experience *block-fading*. The assumption is valid when the considered system is in a quasi-static environment, where the nodes are moving slowly enough such that the channel coherence time exceeds one BD frame duration.

We consider a scenario where the nodes of interest are placed in the Cartesian reference frame of a two-dimensional Euclidean space, as shown in Figure 2.4. The $\lceil N_r/2 \rceil$ AmBC receiver antenna is selected as the reference antenna unless otherwise specified, where $\lceil \cdot \rceil$ is the ceiling function. The line segment connecting the TX antenna and the RX reference antenna is the x-axis, and its midpoint is the origin. The y-axis is parallel with the linear RX array. The locations of the TX, the BD and n_r-th RX antenna are denoted by $\boldsymbol{p}_t$, $\boldsymbol{p}$ and $\boldsymbol{p}_{r,n_r}$, respectively. The distances of TX–n_r-th RX antenna[3], BD–n_r-th RX antenna and TX–BD are in respective order

[3]The notation of A–B denotes from node A to node B.

represented by

$$d_{0,n_r} = \|\boldsymbol{p}_t - \boldsymbol{p}_{r,n_r}\|, \quad d_{1,n_r} = \|\boldsymbol{p} - \boldsymbol{p}_{r,n_r}\|, \quad \text{and} \quad d_2 = \|\boldsymbol{p}_t - \boldsymbol{p}\|. \tag{2.3}$$

For notational simplicity, the distances from the TX and from the BD to the RX reference antenna are denoted as d_0 and d_1, respectively. The distances of the considered system are normalized with respect to the wavelength λ so that the system is frequency-independent, where $\lambda = c_0/f_c$, c_0 is the free-space electromagnetic propagation speed and f_c is the carrier frequency.

Let vectors $\tilde{\boldsymbol{h}}_d \in \mathbb{C}^{N_r \times 1}$, $\tilde{\boldsymbol{h}}_r \in \mathbb{C}^{N_r \times 1}$, and $\tilde{h}_t$ be the channel gains of TX–RX array, BD–RX array, and TX–BD, respectively. The components of $\tilde{\boldsymbol{h}}_d$ are phasor sums of all multi-path components falling in the single tap that are not affected by the operation of the BD modulator. The large-scale spatial average of TX–n_r-th RX antenna can be calculated using the deployment geometry and free-space path-loss model as

$$[\tilde{h}_d]_{n_r} = \rho_0 \frac{\lambda}{4\pi d_{0,n_r}} \exp\left(j2\pi \frac{d_{0,n_r}}{\lambda}\right), \tag{2.4}$$

where ρ_0 is the fading loss of the direct path channel of the current fading block.

For the backscatter path, the propagation paths of an RF signal impinging on the BD antenna are forced to converge to a point, which reduces the rank of the channel matrix [20], [66]. Such a fact makes the backscatter channel a *keyhole* channel and the keyhole in this case is the BD antenna. The hallmark of the keyhole channel is that the channel is modeled as a concatenation of the channel of transmitter–keyhole and the channel of keyhole–receiver, that is

$$[\tilde{h}_b]_{n_r} = \tilde{h}_t [\tilde{h}_r]_{n_r}. \tag{2.5}$$

The components of $\tilde{\boldsymbol{h}}_b$ are phasor sums of all multi-path components that are affected by the BD modulator. Hence, the large-scale spatial average of the backscatter path seen at the n_r-th RX antenna is

$$[\tilde{h}_b]_{n_r} = \rho_1 \frac{\lambda}{4\pi d_2} \frac{\lambda}{4\pi d_{1,n_r}} \exp\left(j2\pi \frac{d_2 + d_{1,n_r}}{\lambda}\right), \tag{2.6}$$

where ρ_1 is the fading loss of the backscatter path. Furthermore, ρ_0 and ρ_1 are independent such that the two channels experience independent fading realizations.

2.3.2 Received Signal

Let $\bar{s}[k]$ be the *narrowband* ambient signal transmitted from the TX at the time instant k with the averaged transmit power $P_s = \mathrm{E}\{|\bar{s}|^2\}$. The noise-free digital sample of the received signal $\tilde{\boldsymbol{y}} \in \mathbb{C}^{Nr\times 1}$ at time instant k is written as

$$\tilde{\boldsymbol{y}}[k] = \tilde{\boldsymbol{h}}_d e^{j\phi_0}\bar{s}[k] + \sqrt{\alpha}\tilde{\boldsymbol{h}}_b e^{j(\phi_0+\phi)}\bar{s}[k]x[k], \tag{2.7}$$

where ϕ_0 is the phase shift caused by the propagation of the direct path, ϕ is caused by the excess path length of the backscatter path compared to the direct path, and α is the power loss caused by the BD modulator which is introduced in Section 2.2.1.

In order to represent the SNR in terms of the transmit power of the ambient TX while keeping the power difference between the two paths, the channel vectors are normalized with respect to the direct path channel gain vector, that is,

$$\boldsymbol{h}_d = \frac{\tilde{\boldsymbol{h}}_d}{\|\tilde{\boldsymbol{h}}_d\|}, \quad \boldsymbol{h}_b = \frac{\sqrt{\alpha}\tilde{\boldsymbol{h}}_b}{\|\tilde{\boldsymbol{h}}_d\|}, \tag{2.8}$$

where $\boldsymbol{h}_d$ and $\boldsymbol{h}_b$ are referred to as the direct path channel and the backscatter path channel, respectively.

At the AmBC RX array, the k-th digital sample of the received signal $\boldsymbol{y} \in \mathbb{C}^{Nr\times 1}$ is given by

$$\boldsymbol{y}[k] = \boldsymbol{h}_d e^{j\phi_0}\bar{s}[k] + \boldsymbol{h}_b e^{j(\phi_0+\phi)}\bar{s}[k]x[k] + \boldsymbol{\omega}[k], \tag{2.9}$$

where $\boldsymbol{\omega} \sim \mathcal{CN}(\mathbf{0}, \boldsymbol{I}_{N_r})$ is the additive circularly-symmetric complex Gaussian noise whose components are independent of x and s. Since the noise has the unit variance and the channels are normalized, the average received SNR of the ambient signal per RX antenna is defined as

$$\gamma = \mathrm{E}\{\|\boldsymbol{h}_d\bar{s}\|^2/N_r\} = P_s/N_r, \tag{2.10}$$

while the total SNR of the ambient signal is equal to P_s. As such, the ambient signal can be represented by the observed SNR γ and the number of RX antennas N_r. The ambient signal is then defined as

$$s = \sqrt{\gamma N_r}\frac{\bar{s}}{|\bar{s}|}e^{j\phi_0}. \tag{2.11}$$

Including the propagation of the direct path ϕ_0 in s is equivalent to taking the timestamp of receiving the ambient signal as the reference. This can be done because demodulating ambient signal accurately is not of interest in an AmBC system. To this point, the received signal can be written as

$$\boldsymbol{y}[k] = \boldsymbol{h}_d s[k] + \boldsymbol{h}_b e^{j\phi}s[k]x[k] + \boldsymbol{\omega}[k], \tag{2.12}$$

and the problem hitherto is improving the performance of demodulating x from the received signal $\boldsymbol{y}$. In the following, the time dependence of $\boldsymbol{y}$ is occasionally dropped when the content is restricted to a single temporal measurement sample.

For an AmBC system that operates under an uncooperative ambient system, the ambient signal is not known at the AmBC receiver. In this case, AmBC receiver design problems should be solved by assuming a certain type of ambient signal. In this work, two types of ambient signal are considered. The worst case is when the AmBC receiver has no prior knowledge about the ambient signal, so it is treated as a deterministic-unknown parameter. The other case is when the receiver assumes a prior distribution for the ambient signal, that is, a zero-mean Gaussian with constant variance. This prior distribution arises in many practical ambient signal sources with fast amplitude variation, such as orthogonal frequency division multiplexing (OFDM) ambient sources.

2.4 Challenges and Available Solutions

This section first gives an explanation of why demodulation of a BD signal in AmBC systems is challenging and then, reviews available solutions in the literature.

2.4.1 Challenges

One factor that hampers the receiver performance is the strong DPI. It is caused by the tremendous power degradation experienced by the backscatter path signal compared to the direct path signal. An example of propagation loss with regard to the backscatter path of an AmBC system operating at $f_c = 500$ MHz is shown in Figure 2.5, where the path-loss exponent is set to 2. In this case, the ambient signal experiences only 46.83 dB propagation loss whereas the BD signal losses are between 80 to 110 dB. Such a difference arises from the extra $\lambda/4\pi$ term in Eq. (2.6). These values indicate that the backscatter signal is significantly weaker compared to the strength of the direct path signal, and has a low signal-to-noise-plus-interference (SINR). On the other hand, the result shows that the SINR of the backscatter signal can be improved by placing the BD close to either the TX or RX.

The strong DPI brings forth a requirement on the dynamic range of

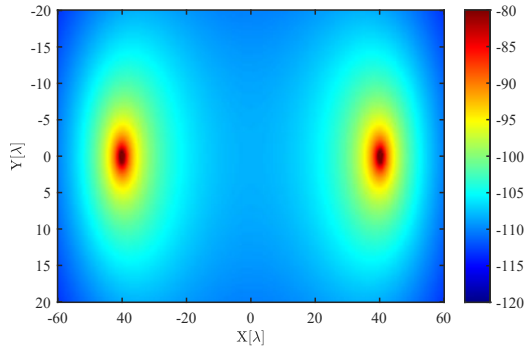

Figure 2.5. Variation in propagation loss in dB of the backscatter path at the RX reference antenna with the BD location when the TX is placed at (-40, 0) and the $\lceil N_r/2 \rceil$-th RX antenna is placed at (40, 0) and the wavelength λ is 0.6 m.

an analog-to-digital converter (ADC) that is implemented on AmBC receivers. Due to the power difference, a digital value of the received signal is dominated by the direct path signal, while the backscatter signal is limited to the least significant bits. Therefore, the ADC dynamic range needs to be high enough for successfully reception of BD signals. Otherwise, suppressing DPI in the analog domain is necessary to alleviate the requirement [67].

The other factor that degrades AmBC receiver performance is due to non-cooperative ambient systems. The rapidly varying and unknown ambient signal has a similar effect as a fast fading on the backscatter signal. These two factors degrade the effective SNR of the backscatter signal, which is the main reason for poor receiver performance.

2.4.2 Solutions

Solutions for improving the receiver performance of demodulating BD signals have been widely investigated. Similar to traditional BC systems, BDs often perform OOK that either backscatters or absorbs ambient RF signals. This gives rise to a variation in received signal strength as the BD switches its states, which intuitively calls for energy-based receivers [11], [19], [31], [68], [69]. Moreover, differential coding can be utilized to eliminate the need of channel estimation [70], [71]. The energy detector is non-coherent so that is does not require tracking unknown ambient signal and channels but averages out the fast varying phase before comparing two signal strength levels. However, when the AmBC receivers have one antenna, the energy detector suffers an error floor problem [71], [72], that is, the probability of error converges to a non-zero value as the transmit

power of the ambient signal goes to infinity.

Canceling DPI can free AmBC receivers from the error floor problem [72], and drastically increase the SINR of the backscatter signal. It is an important step for enhancing AmBC receiver performance which has been used in many AmBC receiver designs. Methods for it are based on specific deployment scenarios. The DPI is canceled using successive interference cancellation (SIC) which jointly detects the ambient signal and BD signal assuming the channel coefficients are available [73]. By introducing a polarization-based BD modulator, the AmBC receiver can differentiate two paths of the signal according to polarizations [74], [75]. Considering FSK-modulated BD signals, the backscatter signal is shifted away from DPI to a higher band [56] or to the guard bands between OFDM symbols [76] such that DPI can be filtered out, or by using the repeating structure of the cyclic prefix in OFDM systems [73]. Another approach facilitating DPI cancellation is using multi-antenna receivers to explore the spatial difference between the direct path signal and the backscatter path signal [19], [53], [77], [78]. This method does not require extra assistance from ambient systems or information on channels. Therefore, adopting multi-antenna receivers in AmBC systems offers greater flexibility and practicality for improving performance.

The attractive advantages of multiple antennas have motivated several works in receiver designs. BD signals can be demodulated from variations in received signal strength [33], [79] or variations in phase [80] on different antenna elements. These works utilize the spatial diversity of the received signal on multiple antennas but lose the array gain potentially provided by the receiver array. The receiver proposed in [77] obtains the array gain by investigating the maximum eigenvalue of the auto-correlation matrix. However, it suffers from an error floor. Moreover, these works consider BDs performing OOK. In terms of receiver performance, OOK needs a higher SNR to achieve the same performance as other modulation which has a larger distance between constellation points. For example, BPSK reaches the performance of OOK with 6-dB less SNR [81, Chapter 4]. BD modulations with a bigger distance between constellation points are as such worth applying to improve receiver performance.

The gain provided by the BPSK modulation is fully achieved by implementing a coherent receiver. Compared with non-coherent receivers that average out unknown phases, coherent receivers have no a phase ambiguity, and thus can achieve the SNR gain. Designing coherent receivers

for AmBC systems requires complex phase synchronizations because the phase of ambient signal and the phase of channels, and the phase offset between the direct path channel and backscatter path channel are all unknown. A coherent receiver proposed in [21] depends on channel state information. A semi-coherent receiver proposed in [56] considers that the ambient signal is unknown and the BD uses frequency-shift-based BPSK modulation. The receiver resorts to shifting the frequency band of the BD signal for DPI cancellation and it needs an ensemble of samples to demodulate one BD signal. Although the unknown phases of channels can be estimated blindly using the expectation maximization (EM) based channel estimation algorithm [82], it requires prior information on ambient signal constellation. Since they require additional information on the legacy system, their practical use is limited. Hence, coherent receivers tackling unknown phases in AmBC systems need to be studied.

ML-assisted demodulation methods are proposed since they relax receivers from estimating intractable unknowns. Some methods infer the BD signal by learning patterns of received signal during transmission of BD training sequences. A demodulator using the expectation maximization algorithm to retrieve the OOK-modulated BD signal is proposed in [83]. The method studied in [30] extracts a unique slope feature from the received WiFi signal. Compared to these methods, the ML-assisted coherent receiver and a deep transfer-learning-based method [18] neither require knowing the constellation of the ambient signal nor restricts the type of the ambient signals. However, deep transfer learning methods can have a high computational complexity.

Even though a coherent receiver for BPSK modulation provides an SNR gain, it comes at the cost of solving several other practical problems and does not generalize well to all AmBC deployment conditions. For example, receiver symbol synchronization is more difficult for BPSK modulation than it is for OOK modulation. Therefore, different BD modulation techniques would require implementing different receivers, which restrains system flexibility. In this regard, having a generalized receiver that can support various binary-modulated signals is desirable. The optimum multi-antenna receiver for the binary-modulated backscatter signal for a Gaussian-distributed ambient signal has already been presented in [77], where the situation without prior information of the ambient signal needs further studies.

Other solutions of increasing the reliability and/or communication range

of the AmBC system include adopting multiple antennas at BDs. It is shown that multiple antennas can mitigate the deep fading of the BD signal in a conventional BC deployment [20]. The multiple BD antenna elements can form communication schemes to facilitate BD transmission. For instance, some antennas constantly harvest the energy to support BD operations, while the optimal antenna [65] or the other group of antennas [84] transmits the BD signal. Applying an orthogonal space-time block coding scheme at multi-antenna BDs also improves receiver performance [21]. The work [35] presents a printed BD array that achieves gigabit data rate communication in a mono-static scenario. In the above studies, BD antennas modulate signals individually without signal transfer between different antennas. As pointed out in [20], signal transfer gives a higher degree of freedom for BD designs and potentially further improves receiver performance. Optimizing modulation on multiple BD antennas hence needs to be investigated.

Applying channel coding is an essential way of improving AmBC receiver performance, and in turn, enlarging the coverage area of AmBC systems as they increase the effective SNR of the backscatter signal [81, Chapter 7]. The repetition code is commonly performed in prior studies. Using an alternative zero-one sequence and an all-zero sequence, the receiver in [33] can avoid synchronization with the BD. These coding schemes require redundant bits due to their poor error-correcting performance [85]. Error-correction coding techniques have also been utilized. High-rate and low-complexity channel coding schemes are used considering the limited energy on BDs while the interleaving technique is applied to further tackle the deep fade channel condition [86]–[88].

2.5 Discussion

This chapter provides an overview of AmBC systems with descriptions of different configurations and BD modulations. The flexibility brought by bi-static configuration, the efficiency of spectrum usage brought by non-frequency shift modulation, and their ability to improve AmBC system performance lead to the system model considered in the thesis.

The backscatter signal power only considers propagation-related losses and BD modulator circuitry loss. Other parameters affecting backscatter signal strength are identified in [15] including the TX and RX antenna gains, BD antenna gain and the polarization mismatch of the links between

TX and BD, and RX and BD. In the theoretical study, we make the following simplifying assumptions: i) TX, RX, and BD have ideal isotropic antennas with unity gain; ii) the links between the TX and BD, and BD and RX polarization mismatches are ignored by assuming perfect polarization matching; and iii) the implementation is close to ideal. Since the considered system is the same as bi-static and dislocated BC systems studied in [15], under these assumptions, the link budget of the backscatter signal is mainly defined by the propagation losses. The effects of other parameters can be included by adding/subtracting to the logarithmic propagation losses. For instance, the impact of transmission power and antenna gains can be added to the logarithmic propagation losses. If there is a polarization mismatch, the amount of the mismatch can be taken into account by substracting a positive number.

The channel model considers the unresolvable multi-path components that fall into a single tap. This is customary for a narrowband system. The designs presented in Chapter 3 follow this assumption such that they can be directly applied to the AmBC system which is implemented under the illumination of narrowband ambient systems, such as LoRa and narrowband-IoT. On the other hand, it also can be generalized to a wideband ambient system, which has been done in Publication VII. To avoid dealing with the wideband channel exhibiting frequency selective fading, one can extract and analyze the signal falling in an individual subcarrier, or consider the signals falling in multiple subcarriers which provides frequency diversity. The practical implementation presented in Chapter 4 adopts the method and shows its feasibility.

Given the system model and the problem of improving BER performance in AmBC systems, the challenges are identified and available solutions are reviewed in this chapter. Specific demodulation methods alluded to thus far need to be tailored to different deployment parameters such as the type of ambient signal and the type of BD modulation. This thesis, on the contrary, considers more generalized assumptions. Specifically, two types of ambient signal assuming with or without prior knowledge are considered. They cover multiple realistic ambient sources, and can be useful for AmBC deployments. In addition, BDs are assumed with general binary ASK and PSK. Therefore, the considered AmBC systems adapt to different practical scenarios and can reduce the dependence of the methods developed in Chapter 3 on specific system setups.

3. Bit Error Rate Performance Optimization

This chapter presents AmBC receivers and BD signaling matrix designs to improve the performance of BD signal demodulation. The criterion of optimum applied throughout this thesis is first described. Two receivers are then introduced, and their performance is analyzed and compared. Finally, a design of BD signaling matrix is presented. This chapter is summarized from Publication II, Publication III, Publication V, and Publication VI.

3.1 Demodulation Criterion

In detection theory, the maximum likelihood criterion arises naturally from the likelihood ratio test, which, according to the Neyman-Pearson Theorem, maximizes the probability of detection for a given probability of false alarm [22, Section 3.3]. It indicates that when the prior information is not assigned, the maximum likelihood criterion gives an optimum receiver. The Bayesian approach can be derived when the prior probabilities of each hypothesis are assigned, as is commonly the case in communication systems. This yields the maximum-a-posteriori (MAP) criterion which minimizes the Bayesian risk and is optimum (also referred to as the *strongest*) binary hypothesis test although it does not require a specified false alarm probability to maximize the probability of detection. Therefore, we apply the MAP criterion to obtain optimal designs. The derived receivers are optimal in the Bayesian sense and have the lowest probability of error among all possible binary hypothesis tests.

Let $\mathcal{H}_0$ and $\mathcal{H}_1$ denote the *null-hypothesis* and its alternative hypothesis. For a binary-modulated signal $x \in \{x_0, x_1\}$, we have $\mathcal{H}_i : x = x_i, i = 0, 1$ is transmitted. The binary hypothesis test selecting the hypothesis based on MAP criterion is

$$\Pr(x_0|\boldsymbol{y}) \underset{\mathcal{H}_1}{\overset{\mathcal{H}_0}{\gtrless}} \Pr(x_1|\boldsymbol{y}), \tag{3.1}$$

where $\Pr(x_i|\boldsymbol{y}), i = 0, 1$ is the posterior probability of the BD signal x_i given a received signal $\boldsymbol{y}$. For a random vector $\boldsymbol{y}$ with a probability density function (PDF) $f(\boldsymbol{y})$, the posterior probability can be computed using Bayes' theorem

$$\Pr(x_i|\boldsymbol{y}) = \frac{f(\boldsymbol{y}|x_i)\Pr(x_i)}{f(\boldsymbol{y})}. \tag{3.2}$$

Since the denominator is the same under two hypotheses, the MAP criterion can be rewritten as

$$f(\boldsymbol{y}|x_0) \underset{\mathcal{H}_1}{\overset{\mathcal{H}_0}{\gtrless}} \frac{\Pr(x_1)}{\Pr(x_0)} f(\boldsymbol{y}|x_1), \tag{3.3}$$

where $f(\boldsymbol{y}|x_i)$ is the likelihood function of $\boldsymbol{y}$ given x_i is transmitted.

The hypothesis testing yields a test statistic z and a decision threshold V. Once the distribution of z is determined, the performance of a receiver is quantified by the probability of error P_e which is the average of the probability of false alarm (also known as Type-I error) P_f and the probability of miss (also known as Type-II error) P_m. For a problem at hand, these probabilities are given by

$$\begin{gathered} P_f = \Pr(\mathcal{H}_1|\mathcal{H}_0) = 1 - F_z(V|x_0), \quad P_m = \Pr(\mathcal{H}_0|\mathcal{H}_1) = F_z(V|x_1), \\ P_e = \Pr(x_0) \cdot P_f + \Pr(x_1) \cdot P_m, \end{gathered} \tag{3.4}$$

where $\Pr(\mathcal{H}_i|\mathcal{H}_j)$ denotes the probability of deciding $\mathcal{H}_i$ but $\mathcal{H}_j$ is true and $F_z(\cdot|x_i)$ is the conditioned cumulative distribution function (CDF) of the test statistic z. Therefore, given a test statistic and its distribution and a decision threshold, one can quantize the probability of error of a receiver.

3.2 Coherent Receiver Design

A coherent receiver can provide an SNR gain by not averaging over an unknown phase, even though this is at the cost of phase synchronization. It is challenging in AmBC systems since the phases of ambient signal and channels are all unknown at the receiver. This section presents that a multi-antenna receiver is able to address these difficulties, and the proposed AmBC coherent receiver realizes the phase estimation and compensation, which is studied in Publication II and Publication III.

In the system model depicted in the last chapter, the backscatter signal traverses an excess path length compared to the direct path signal. The excess path length causes a phase offset denoted by ϕ, as indicated in Eq. (2.12), which varies with the BD location. One realization of the phase offset variation as a function of the BD location is illustrated in Figure 3.1.

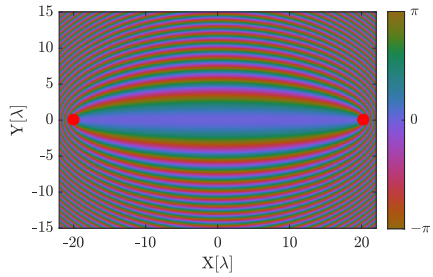

Figure 3.1. Variation in the phase offset ϕ with the BD location when the direct path length $d_0 = 40\lambda$, and the phase difference between the random small-scale fading of two paths, i.e., ρ_0 and ρ_1, is 0. The red circles represent the TX and the reference antenna of AmBC RX.

As can be seen, a small change in the location leads to a large variation in ϕ. The variation in ϕ is particularly high when the BD is in the close vicinity of the TX and the RX. In what follows, it is shown that the phase offset plays an important role in demodulating a BD signal and cannot be ignored.

3.2.1 Receiver Structure

The backscatter path channel can be decomposed as $\boldsymbol{h}_b = \eta_1 \boldsymbol{h}_d + \eta_2 \boldsymbol{c}$, where $0 \leq \eta_1, \eta_2 \leq 1$ are the projections of $\boldsymbol{h}_b$ onto $\boldsymbol{h}_d$ and $\boldsymbol{c}$, respectively. The direction $\boldsymbol{c}$, defined as

$$\boldsymbol{c} = \frac{(\boldsymbol{I} - \boldsymbol{h}_d \boldsymbol{h}_d^H)\boldsymbol{h}_b}{\|(\boldsymbol{I} - \boldsymbol{h}_d \boldsymbol{h}_d^H)\boldsymbol{h}_b\|}, \tag{3.5}$$

indicates the component of the backscatter path channel that is orthogonal to the direct path channel. As such, the received signal in Eq. (2.12) can be rewritten as

$$\boldsymbol{y} = \boldsymbol{h}_d s + (\eta_1 \boldsymbol{h}_d + \eta_2 \boldsymbol{c}) e^{j\phi} s x + \boldsymbol{\omega}. \tag{3.6}$$

Pre-processing

The DPI is firstly canceled by projecting the received signal into the null space of the direct path channel. It gives the residual signal

$$\boldsymbol{r} = (\boldsymbol{I} - \boldsymbol{h}_d \boldsymbol{h}_d^H)\boldsymbol{y} = \eta_2 \boldsymbol{c} e^{j\phi} s x + (\boldsymbol{I} - \boldsymbol{h}_d \boldsymbol{h}_d^H)\boldsymbol{\omega}. \tag{3.7}$$

The strongest signal direction of the residual signal is in the direction $\boldsymbol{c}$ defined in Eq. (3.5). Combining the residual signal using the direction $\boldsymbol{c}$ gives the *effective backscatter signal* as

$$u = \boldsymbol{c}^H \boldsymbol{r} = \boldsymbol{c}^H \boldsymbol{y} = \eta_2 e^{j\phi} s x + \boldsymbol{c}^H \boldsymbol{\omega}, \tag{3.8}$$

where $\boldsymbol{c}^H\boldsymbol{\omega} \sim \mathcal{CN}(0,1)$ is the projection noise, and we define

$$\gamma_e = P_s|\eta_2|^2 = P_s(\|\boldsymbol{h}_b\|^2 - |\boldsymbol{h}_b^H\boldsymbol{h}_d|^2) \tag{3.9}$$

as the effective SNR of the backscatter signal.

ML-Assisted Coherent Receiver

Given the effective backscatter signal u, the receiver derived from the MAP criterion is given by [89, Chapter 4]

$$\mathrm{Re}\{e^{-j\phi}\hat{s}^* u\} = \mathrm{Re}\{e^{-j\phi}\boldsymbol{y}^H\boldsymbol{h}_d\boldsymbol{c}\boldsymbol{y}\} = \cos\phi \cdot \mathrm{Re}\{z_t\} + \sin\phi \cdot \mathrm{Im}\{z_t\}, \tag{3.10}$$

where $\hat{s} = \boldsymbol{h}_d^H\boldsymbol{y}$ and

$$z_t = \hat{s}^* u = \boldsymbol{y}^H\boldsymbol{h}_d\boldsymbol{c}^H\boldsymbol{y}. \tag{3.11}$$

It is worth noting that the receiver does not need prior information on the ambient signal. Instead, it utilizes the multi-antenna RX to estimate the ambient signal.

The resultant test statistic implies the optimum receiver is a correlation receiver [89, Section 4.4]. It is affected by the phase offset ϕ caused by the excess path length, which is unknown to the receiver. The calculated data z_t of two length of $L = 50$ BD sequences is shown in Figure 3.2a. The two BD sequences are $x = -1$ (blue square) and $x = +1$ (red cross) respectively, and s follows Gaussian distribution. The unknown ϕ brings a rotation to the data z_t. A coherent correlation receiver estimates the unknown ϕ and compensates for it. Then, the decisions are made by comparing the real part of the rotated z_t to the threshold 0, i.e., the decision boundary is the imaginary axis. Nevertheless, due to the low SNR of the backscatter signal, the unknown ambient signal and the unknown BD location, it is challenging to estimate the phase offset ϕ and compensate for it. Several calibration techniques for ϕ are proposed in [90] which rely on the pilots transmitted from ambient systems. On the other hand, ignoring ϕ but only considering $\mathrm{Re}\{z_t\}$ degrades the receiver performance. An extreme case arises when $\phi = \frac{\pi}{2}$, which yields the sufficient test statistic to be $\mathrm{Im}\{z_t\}$. Therefore, the unknown ϕ needs to be compensated.

As shown in Figure 3.2a, data z_t of two BD sequences in which $x = -1$ and $x = 1$, respectively, falls into two clusters, motivating us to use an ML classification to classify two classes. The ML-assisted method implicitly compensates for the impact of ϕ via learning the pattern of z_t. It is equivalent to rotating the complex plane to separate z_t, and thus, it is equivalent to the optimum correlation receiver. Therefore, the test

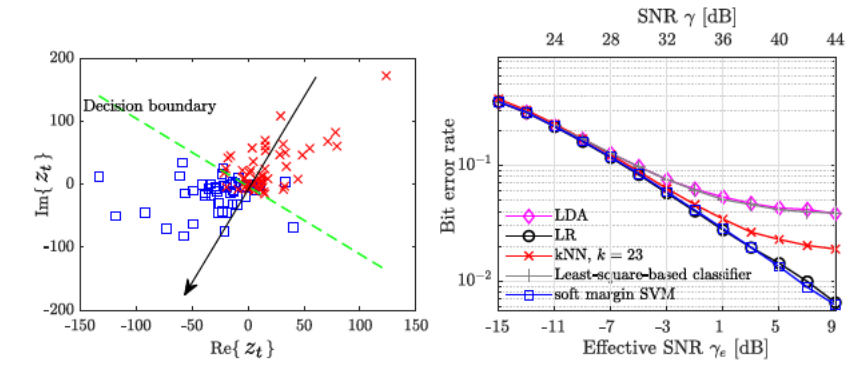

Figure 3.2. In (a), visualization of two length of $L = 50$ BD sequences within one channel coherence time. In (b), variation in AmBC BER as a function of effective SNR γ_e for $L = 64$ with different markers for different ML classifiers.

statistic of the ML-assisted coherent receiver is z_t in Eq. (3.11). The real and the imaginary parts of z_t are utilized as features, and a data set of $[\mathrm{Re}\{z_t\}, \mathrm{Im}\{z_t\}]$ conditioned on known BD symbols that are transmitted for a certain duration, referred to as the ***preamble***, is utilized as the training set to calculate the decision boundary. The rest of the transmitted symbols are classified by comparing their test statistics with the decision boundary.

The data set belonging to two classes is overlapping, shown in Figure 3.2a, due to the low SNR of the backscatter signal. As the SNR increases, the overlapping area diminishes. However, it will not disappear according to the data distribution, which is analyzed in Publication III. Hence, both linear and nonlinear classifiers can be used for the demodulation.

The selection of a classifier depends on its performance as well as the computational requirements, and the length of the training data. Linear classifiers including the logistics regression (LR), the soft margin support vector machine (SVM), the linear discriminant analysis (LDA), the least-square-based classifier, and a simple nonlinear classifier, the k-nearest neighbor (kNN), are candidates for learning the pattern. Among these algorithms, the soft margin SVM can be configured by using a hyperparameter to control the weight of the soft margin latent variables, which, in turn, defines how well it fits the training data. Although the SVM and LR have similar cost functions, the LR casts the fitting problem using the Sigmoid function and looks at the probabilities of an observation being in either of the classes. The SVM has similar performance to the LR when its hyperparameter is adjusted. The least-squares-based classifier obtains the parameters by minimizing the prediction error, and LDA obtains the

parameters by maximizing the class separation. However, for predicting the BPSK-modulated signal with equal probability, they are equivalent to each other [91]. The kNN classifies data intuitively by assigning it to the class which has the majority votes among k selected nearest neighbors.

An example of BER performance of different classifiers as a function of the effective SNR γ_e is shown in Figure 3.2b. All classifiers have an indistinguishable performance in the low SNR region. In the high SNR region, the soft margin SVM and the LR still have similar performance, and they outperform the others. The LDA and the least-square classification also perform similarly, but compared with the SVM and the LR, they lack robustness against the outliers. Also, the assumption of the LDA that the observations of each class follow a Gaussian distribution is not applicable to the studied case. On the other hand, the kNN has acceptable performance. It can be highly accurate with a large training size and for a carefully adjusted number of neighbors parameter k. However, this requirement cannot be always satisfied since short preambles should be designed in order to save BD energy. Furthermore, a large preamble size and k also introduce a high computational burden and a higher memory requirement. Consequently, the LR classifier is the most suitable for mitigating the impact of the unknown phase offset ϕ.

Conventional receivers

For comparison, two conventional receivers derived from the effective backscatter signal u are also provided in Publication III. One is the coherent receiver with perfect knowledge of the phase offset ϕ. The test statistic of the coherent receiver is given by

$$z_c = \mathrm{Re}\{e^{-j\phi}\boldsymbol{y}^H\boldsymbol{h}_d\boldsymbol{c}^H\boldsymbol{y}\} = \boldsymbol{y}^H\left(\frac{e^{-j\phi}\boldsymbol{h}_d\boldsymbol{c}^H + e^{j\phi}\boldsymbol{c}\boldsymbol{h}_d^H}{2}\right)\boldsymbol{y} \triangleq \boldsymbol{y}^H\boldsymbol{M}_c\boldsymbol{y}. \quad (3.12)$$

The decision threshold is derived based on the MAP criterion given the distribution of z_c. The coherent receiver with a known ϕ achieves the SNR gain whose performance is the lower bound for the ML-assisted coherent receiver.

Another typical receiver is a non-coherent energy receiver. It requires statistical information on the unknown parameters. The receiver marginalizes over unknown parameters, i.e., the ambient signal s and the phase offset ϕ, in the effective backscatter signal u defined in Eq. (3.8). This yields an energy receiver that measures the energy of the effective backscatter signal $z_n = |u|^2$. For this non-coherent energy receiver, only an ASK-modulated BD signal can be demodulated. For example, when the backscatter signal

is OOK-modulated, the receiver tests the presence of the backscatter signal against the absence of it.

3.2.2 Performance Analysis

Probability of error derivation

In order to quantize the performance of the ML-assisted coherent receiver, we consider the coherent receiver in Eq. (3.12) with perfect knowledge of ϕ, which provides a lower bound of the probability of error. We further assume the receiver has perfect knowledge of the two directions $\boldsymbol{h}_d$ and $\boldsymbol{c}$. As is derived in Publication III, the distribution of z_c conditioned on x_i follows the asymmetric Laplace distribution with the location parameter 0, the scale parameter $-\sqrt{-1/[\mu_1(x_i)\mu_2(x_i)]}$ and the asymmetry parameter $\sqrt{-\mu_1(x_i)/\mu_2(x_i)}$ [92, Chapter 3]. The two characteristic parameters $\mu_\ell(x_i),$ for $\ell \in \{1, 2\}$ are two eigenvalues of the matrix $\mathcal{M} = \boldsymbol{\Sigma}_{\boldsymbol{y}|x_i}\boldsymbol{M}_c$, and $\boldsymbol{\Sigma}_{\boldsymbol{y}|x_i}$ is the covariance matrix of the received signal $\boldsymbol{y}$ conditioned on x_i, and $\boldsymbol{M}_c$ is defined in Eq.(3.12). Given the conditional distribution, the probability of error of the receiver is calculated using Eq. (3.4).

Key parameters

The expectation and the variance of z_c conditioned on x_i are $\mathrm{E}\{z_c|x_i\} = -\mu_2(x_i) - \mu_1(x_i)$ and $\mathrm{Var}\{z_c|x_i\} = \mu_2^2(x_i) + \mu_1^2(x_i)$, respectively. For a practical AmBC system, the eigenvalues can be approximated by

$$\mu_\ell(x_i) \approx \mathrm{Re}\{\frac{P_s}{2}\eta_2 x_i^*\} + (-1)^\ell \frac{\sqrt{P_s}}{2}. \tag{3.13}$$

By using this approximation of the eigenvalues, z_c conditioned on x_0 and x_1 have opposite expectations and similar variances. As we known from the properties of the asymmetric Laplace distribution, the overlap between the data set belonging to the two classes will not disappear. It diminishes as the difference between the two expectations enlarges, which, in turn, improves the BER performance. The expectation is approximated as $\mathrm{E}\{z_c|x_i\} \approx -\mathrm{Re}\{P_s\eta_2 x_i^*\}$. Therefore, the BER performance can be improved by increasing the total SNR of the ambient signal or by having a strong backscatter path component that is orthogonal to the direct path.

The power difference between the effective backscatter signal and the direct path signal can be defined as $\Delta_e = \gamma_e/P_s = |\eta_2|^2$. This indicates that the power difference is a function of BD location. An example of variation in Δ_e as a function of BD location is shown in Figure 3.3. When the BD is far away from both the TX and the RX, the backscatter path undergoes a

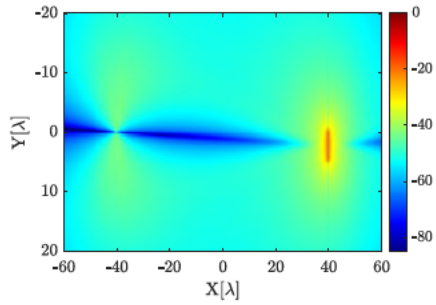

Figure 3.3. Variation in the power difference between direct path and effective backscatter path Δ_e as a function of BD location for direct path length $d_{01} = 80\lambda$, number of antennas $N_r = 10$ and $\alpha = 0.6$. In this figure, the first AmBC RX antenna is set as the reference antenna.

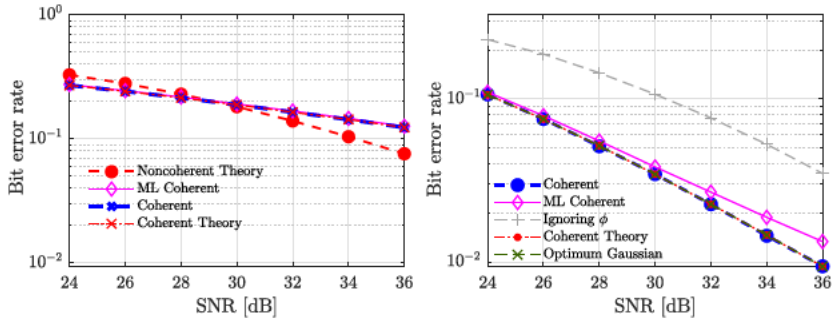

(a) **(b)**

Figure 3.4. Variation in AmBC BER as a function of the SNR of the ambient system γ with different markers for different receivers when the BD performs (a) OOK, and (b) BPSK. *Theory* in the legend denotes the theoretical probability of error of a receiver.

tremendous power loss, nearly -60 dB. Even with a short distance $d_{11} \approx 2\lambda$, Δ_e reaches over -40 dB. The result implies that the effective SNR of the backscatter signal is usually less than 0 dB even when the total SNR of the ambient signal is 30 dB. Moreover, there exists a null beam on the line segment between the TX and the RX. One can predict that the receiver fails to detect the backscatter signal when the BD is placed in the null beam as η_2 is extremely small. However, the null beam will become narrower as N_r increases.

3.2.3 Performance Evaluation

For evaluating the receivers, the distance of TX–RX is $d_0 = 80\lambda$. The BD is placed at $p = [40\lambda - d_1/\sqrt{2}, d_1/\sqrt{2}]$ with $d_1 = 4\lambda$. Receiver performance is represented in terms of BER, while if a coding scheme is used for the BD signal, it is represented by symbol error rate (SER).

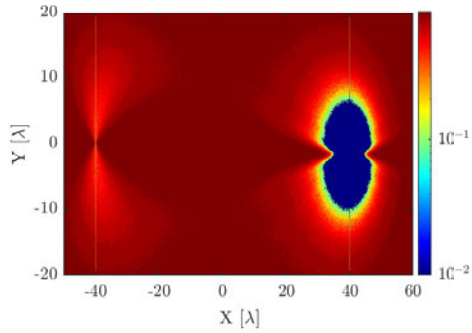

Figure 3.5. Variation in AmBC Symbol-Error-Rate (SER) in log scale as a function of BD location for $d_{01} = 80\lambda$, code order $r = 3$, and SNR of ambient signal $\gamma = 30$ dB.

Figure 3.4 depicts the BER performance of the proposed receivers including the ML-assisted coherent receiver, the coherent receiver with known phase offset, and the non-coherent energy receiver as a function of the ambient signal SNR γ for both OOK and BPSK and $N_r = 10$. The effective SNR of the backscatter signal in this scenario is $-5.8 \leq \gamma_e \leq 6.2$ dB. The ambient signal samples are generated from zero-mean Gaussian distribution with average transmit power calculated from the SNR of the ambient system. For OOK, the non-coherent energy receiver performs worse in the low SNR region but it outperforms the coherent receiver as the SNR increases. This is because the coherent receiver coarsely estimates the ambient signal whereas the non-coherent energy receiver considers its signal space. It can be observed that BPSK has more than 6-dB gain compared with OOK. The results show that the ML-assisted coherent receiver performance is close to the performance of the coherent receiver with a known ϕ which provides a lower bound of the error probability. Ignoring ϕ degrades the detection performance, where the degradation depends on the BD location. In this considered scenario, ignoring ϕ loses 3-dB from the coherent receiver. Hence, it is necessary to take into account the phase offset, and the proposed ML-assisted receiver sufficiently mitigates its adverse impact.

Variation in SER of the ML-assisted coherent receiver in the log scale for the ambient signal SNR $\gamma = 30$ dB is shown in Figure 3.5. It is noted that the Simplex code[1] with a code rate of 3 is used for the BD signal. The result indicates that the BD is supposed to be placed either in the close vicinity of the TX or a region ($\sim 20\lambda$) around the RX, but not on the line

[1]In this work, Simplex code is selected due to its easy implementation and it achieves the same performance as Hadamard code with one dimension less codewords [93, Chapter 8].

between the TX and RX where the backscatter path and the direct path signals are not separable. The shape of the coverage area close to the RX is due to the symmetric linear antenna array. The figure gives a perspective of the coverage area of one single-antenna BD deployment.

3.3 Optimum Receiver Design

This section presents the optimum receiver investigated in Publication V. Unlike the coherent receiver that takes the direct path channel and the backscatter path channel individually into consideration, the optimum receiver investigates the composite channel. Let $\boldsymbol{g}_i$ denote the composite channel such that a sample of the received signal in Eq. (2.12) reads as

$$\boldsymbol{y} = \boldsymbol{g}_i s + \boldsymbol{\omega}, \quad \text{for } i = 0, 1, \tag{3.14a}$$

$$\boldsymbol{g}_i \triangleq \boldsymbol{g}(x_i) = \boldsymbol{h}_d + \boldsymbol{h}_b e^{j\phi} x_i. \tag{3.14b}$$

In the following derivation, when the content is restricted to a single temporal measurement sample, the time dependence of $\boldsymbol{y}$ is dropped. For an AmBC system where the duration of a BD symbol x is longer than the duration of the ambient symbol s, which is the common scenario, the optimum receiver is assumed to take K oversamples for demodulating one BD symbol, where K refers to the *oversampling rate*. Each temporal sample of the received signal $\boldsymbol{y}$ is affected by independent symbol s. In this case, the time dependence of $\boldsymbol{y}$ and that of s are kept.

The optimum receiver is derived considering both the deterministic-unknown ambient signal and the Gaussian-distributed ambient signal depending on whether there is prior information about s. When the ambient signal s is assumed to be deterministic-unknown, the averaged transmit power is $P_s = |s|^2$, while the averaged transmit power of Gaussian-distributed s is $P_s = \sigma_s^2$, respectively.

3.3.1 Receiver Structure

Deterministic-unknown ambient signal

In case the ambient signal is taken as an unknown constant, it is estimated from a single temporal measurement of $\boldsymbol{y}$. Let $\hat{s}$ denote the estimate of the ambient signal and $\epsilon_s = \hat{s} - s$ denote the estimation error. The measurement is such that having a joint distribution of the estimation error ϵ_s and measurement noise $\boldsymbol{\omega}$. The likelihood function of the measurement

is obtained by marginalizing out the estimation error. It is written as

$$f(\boldsymbol{y}|x_i) = \int_{\mathbb{S}} f(\boldsymbol{y}|x_i, \epsilon_s) f(\epsilon_s) d\epsilon_s, \tag{3.15}$$

where $\mathbb{S}$ is the support of the ambient signal estimation error, and $f(\epsilon_s)$ denotes its PDF. Therefore, the marginal density of ϵ_s and the conditional density are required to find the likelihoods.

The maximum likelihood estimator is selected to estimate the ambient signal as it is an unbiased and efficient estimator [94]. It is worth noting that, when the MAP criterion reduces to the maximum likelihood criterion, using the maximum likelihood estimate to replace the unknown s is the generalized likelihood ratio test approach [22, Chapter 6]. It gives the estimate $\hat{s}$ and the associated estimation error ϵ_s as

$$\hat{s} = \frac{\boldsymbol{g}_i^H \boldsymbol{y}}{\|\boldsymbol{g}_i\|^2}, \quad \epsilon_s = \hat{s} - s = \frac{\boldsymbol{g}_i^H \boldsymbol{\omega}}{\|\boldsymbol{g}_i\|^2}. \tag{3.16}$$

The estimation error ϵ_s is a complex Gaussian random variable with zero mean and variance $\mathrm{E}\{\epsilon_s \epsilon_s^*\} = 1/\|\boldsymbol{g}_i\|^2$. As the number of receiver antennas increases, $\mathrm{E}\{\epsilon_s \epsilon_s^*\} \to 0$, and $f(\epsilon_s) \to \delta(\epsilon_s)$, where $\delta(\cdot)$ is the Dirac delta function. Hence, the estimator is also asymptotically consistent.

Substituting the estimate $\hat{s}$ into Eq. (3.14a) gives

$$\boldsymbol{y} = \hat{s}\boldsymbol{g}_i + \tilde{\boldsymbol{\omega}}, \quad \tilde{\boldsymbol{\omega}} = \left(\boldsymbol{I} - \frac{\boldsymbol{g}_i \boldsymbol{g}_i^H}{\|\boldsymbol{g}_i\|^2} \right) \boldsymbol{\omega} \triangleq \boldsymbol{G}_d(x_i) \boldsymbol{\omega}. \tag{3.17}$$

One can observe that the conditional distribution of measurement given $\hat{s}$ and ϵ_s is a degenerate multi-variate Gaussian with mean $\hat{s}\boldsymbol{g}_i$ and variance $\boldsymbol{G}_d(x_i)$. Even though the PDF of the conditional distribution does not exist in $\mathbb{C}^{N_r}$, it can be defined in a subspace [95, Section 8a.4]. Since the conditional covariance matrix $\boldsymbol{G}_d(x_i)$ is an idempotent matrix of rank $N_r - 1$, the conditional PDF is defined in the $(N_r - 1)$-dimensional subspace.

When the receiver takes K samples for one BD symbol, the received signal samples conditioned on x_i and ϵ_s are independent as the noise samples are independent in time. It follows that the joint density is their respective products. Substituting the conditional PDF into the binary hypothesis testing, the optimum receiver for the deterministic-unknown ambient signal case is given by

$$z_d \triangleq \sum_{k=1}^{K} \boldsymbol{y}^H[k] \left(\boldsymbol{G}_d(x_1) - \boldsymbol{G}_d(x_1) \right) \boldsymbol{y}[k] \underset{\mathcal{H}_1}{\overset{\mathcal{H}_0}{\gtrless}} K \ln \left(\frac{1 - \Pr(x_0)}{\Pr(x_0)} \right) \triangleq V_d, \tag{3.18}$$

where z_d defines its test statistic. In particular, when BD symbols have a equal probability, the decision threshold $V_d = 0$.

Gaussian-distributed ambient signal

The multi-antenna optimum receiver for the Gaussian-distributed ambient signal demodulating the OOK-modulated BD symbol is investigated in [19], [77], which is a generalization of the single-antenna optimum receiver presented in [71]. The performance of the optimum receiver is provided in [23] in terms of BER. Even though it leads to the same receiver structure, unlike [19], [77], Publication V considers the general binary modulated BD signal. In addition, the probability of error derivations in [23] have infinite series, which do not converge for all practical parameter ranges. Publication V presents a probability of error analysis with a closed-form distribution.

The conditional density of a measurement $\boldsymbol{y}$ given a BD symbol $x = x_i$ is Gaussian with mean $\mathbf{0}$ and conditional covariance $\boldsymbol{\Sigma}_{\boldsymbol{y}|x_i} = \sigma_s^2 \boldsymbol{g}_i \boldsymbol{g}_i^H + \boldsymbol{I}$ [96]. For a receiver acquiring K samples for one BD symbol, the joint condition density of measurements is the product of individual samples due to the independence of noise process samples. Substituting in the joint condition densities, the binary hypothesis testing is simplified to

$$\begin{aligned} z_g &\triangleq \frac{1}{K} \sum_{k=1}^{K} \boldsymbol{y}[k]^H \left(\boldsymbol{G}_g(x_1) - \boldsymbol{G}_g(x_0) \right) \boldsymbol{y}[k] \\ &\underset{\mathcal{H}_1}{\overset{\mathcal{H}_0}{\gtrless}} \ln \left(\frac{1 - \Pr(x_0)}{\Pr(x_0)} \frac{1 + \sigma_s^2 \|\boldsymbol{g}_0\|^2}{1 + \sigma_s^2 \|\boldsymbol{g}_1\|^2} \right) \triangleq V_g, \end{aligned} \tag{3.19}$$

where

$$c_i \triangleq \frac{\sigma_s^2 \|\boldsymbol{g}_i\|^2}{1 + \sigma_s^2 \|\boldsymbol{g}_i\|^2}, \qquad \boldsymbol{G}_g(x_\ell) \triangleq \boldsymbol{\Sigma}_{\boldsymbol{y}|x_i}^{-1} = \boldsymbol{I} - c_i \frac{\boldsymbol{g}_i \boldsymbol{g}_i^H}{\|\boldsymbol{g}_i\|^2}. \tag{3.20}$$

3.3.2 Performance Analysis

Probability of error derivation

In order to evaluate the performance of the two receivers, distributions of z_d and z_g are rigorously derived in Publication V. Both test statistics are quadratic forms determined, respectively, by matrices

$$\boldsymbol{M}_d = \boldsymbol{G}_d(x_1) - \boldsymbol{G}_d(x_1), \quad \boldsymbol{M}_g = \boldsymbol{G}_g(x_1) - \boldsymbol{G}_g(x_1), \tag{3.21}$$

whose spectral properties are the parameters formulating the distributions.

The test statistic z_d in the deterministic-unknown case is a difference of two independent non-central chi-square distributions. Although the exact density of such a distribution is given in [97], the resultant density function does not converge for the parameter ranges of interest. It is

proposed in Publication V to consider the ratio of the two non-central chi-square distributions as the alternative test statistic. This ratio results in a doubly non-central F distribution [98, Chapter 30]. While the distribution suffers from slow convergence of calculating the sum [99, Section 10.2], it can be overcome using the saddle point approximation [100].

For the case of a Gaussian-distributed ambient signal, z_g is rewritten as a central quadratic form. It follows the distribution of a sum of independent indefinite Hermitian Gaussian quadratic forms whose density functions depend on the eigenvalues of the Hermitian matrices. The density function is derived as a straightforward extension of the results studied in [101]. Specifically, when $K = 1$, the distribution is the asymmetric Laplace distribution which has been investigated in Publication III.

Equivalence of two optimum receivers

The difference between the receiver for a deterministic-unknown ambient signal in Eq. (3.18) and the receiver for a Gaussian-distributed ambient signal in Eq. (3.19) arises from the coefficients c_i, for $i = 0, 1$. For the deterministic-unknown case, $c_i = 1$. For the Gaussian case, when the total received SNR of ambient signal is high, for example, higher than 20 dB, we have $\sigma_s^2 \|\boldsymbol{g}_i\|^2 > 100$, which implies $c_i \approx 1$. In this case, z_g approximates to z_d. Furthermore, the decision threshold in the Gaussian-distributed case can be written as

$$V_g = \ln\left(\frac{c_1 \|\boldsymbol{g}_0\|^2}{c_0 \|\boldsymbol{g}_1\|^2}\right). \tag{3.22}$$

For all practical AmBC deployments, the channel gains $\boldsymbol{h}_d$ and $\boldsymbol{h}_b$ have a significant gain difference. This implies that $\|\boldsymbol{g}_0\|^2/\|\boldsymbol{g}_1\|^2 \approx 1$, and $V_g = 0$. Therefore, when the total received SNR of the ambient signal is high and the channel gain difference between the direct path and backscatter path is large, the two receivers are equivalent.

Key parameter

The derivation of receiver performance suggests that the performance is improved as parameters P_s and κ increase. The parameter P_s denotes the total received SNR of the ambient signal. The parameter κ, defined as

$$\kappa = \sqrt{1 - \frac{|\boldsymbol{g}_0^H \boldsymbol{g}_1|^2}{\|\boldsymbol{g}_0\|^2 \|\boldsymbol{g}_1\|^2}}, \tag{3.23}$$

indicates the absolute value of sine of the rotation angle between $\boldsymbol{g}_0$ and $\boldsymbol{g}_1$, which takes a real value between 0 and 1. We refer to κ as *angular variation*. It is 0 when the two directions are parallel, and 1 when the

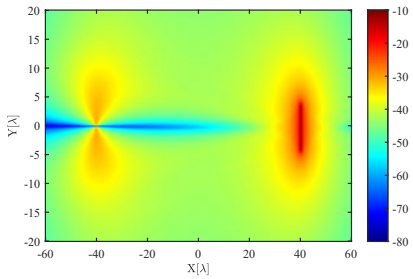

Figure 3.6. Variation in $20\log_{10}(\kappa)$ with BD location when BD performs BPSK, $N_r = 16$.

two directions are orthogonal. Correspondingly, κ attains its maximum when the channel gains $\boldsymbol{h}_d$ and $\boldsymbol{h}_b$ are perpendicular to each other, and its minimum when they are parallel. The two-dimensional variation in κ is shown in Figure 3.6. The depicted result shows that the angular variation is the largest when the BD is close to RX or TX. Therefore, the derived optimum receivers achieve good performance when the BD has a suitable location, and it may perform at its best when the BD is within $\pm 10\lambda$ distance from the RX or close to the TX within approximately $\pm 5\lambda$. Additionally, having a high total SNR of the ambient signal improves performance.

3.3.3 Performance Evaluation

Impact of different system parameters on the BER of the optimum receiver for a BPSK-modulated BD signal is shown in Figure 3.7. The legend uses *ambient signal type – receiver type* notation for numerical results, and probability of error curves are indicated with their names. The impact of the number of receiver antennas N_r and oversampling rate K on the BER of the optimum receiver for Gaussian s is illustrated in Figure 3.7a. An acceptable BER is achieved when $N_r \geq 4$ and $K \geq 4$, and hence, for the following evaluations we fix $N_r = 4$ and $K = 4$. A higher oversampling rate corrects more errors, especially when the BD is placed far away from both the TX and the RX. However, this is achieved at the expense of higher BD transmission power and/or higher RX sampling rate. Therefore, a tradeoff needs to be considered when deciding AmBC system parameters.

The impact of ambient signal modulation on BER performance is shown in Figure 3.7b, where three different ambient signals are studied. When s is Gaussian-distributed, both Gaussian and deterministic receivers have the same performance, which validates that the two receivers are equivalent under certain conditions as discussed in Section 3.3.2. The deterministic

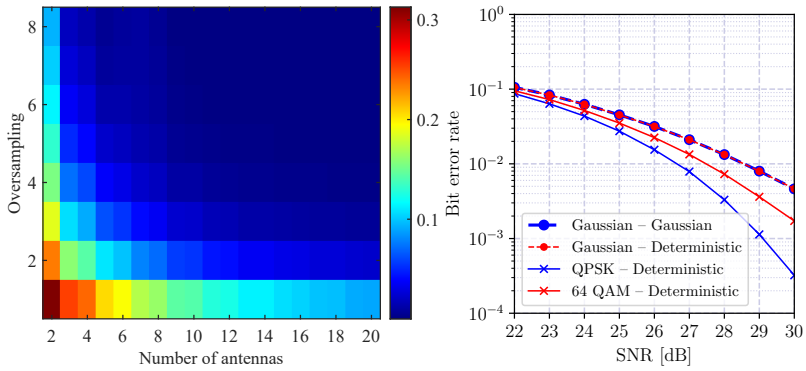

Figure 3.7. In (a), variation in BER of the optimum receiver for Gaussian s with number of receiver antennas N_r and number of samples acquired for each symbol K when the ambient system SNR $\gamma = 24$ dB, BD uses BPSK modulation and the beamformers are perfectly known. In (b), variation in BER as a function of ambient system SNR γ when the ambient signal is Gaussian distributed, 64-QAM and QPSK modulated when BD uses BPSK modulation.

receiver when s is QPSK modulated outperforms that when s is Gaussian distributed. This is because for a Gaussian-distributed s, its amplitude has high variability, whereas for QPSK it is constant. An intermediate case is when s is 64-ary QAM modulated. This modulation introduces some variability on the amplitude of s, but its entropy is smaller than the Gaussian-distributed s case. Correspondingly, M-ary QAM is expected to have the performance close to QPSK modulated s case when M is low, and approaches Gaussian s performance as M increases. Therefore, the deterministic receiver can handle different types of ambient signals, but it has a different performance.

The optimum receiver for different ambient signals and binary modulated BD signals with the SNR of the ambient signal γ are shown in Figure 3.8. For both the OOK-modulated BD signal, shown in Figure 3.8a, and the BPSK-modulated BD signal, shown in Figure 3.8b, the theoretical probabilities of error have the same result as the corresponding BER curves obtained by simulations. Therefore, the derivations of the probability of error are valid, and that for the OOK-modulated BD signal can be used for receivers in the earlier literature to evaluate their expected performance. In particular, since the Gaussian receiver for OOK modulation is the same as the one studied in [77], the benefits of using a BPSK-modulated BD signal and the generality of the proposed receiver are implied by the results.

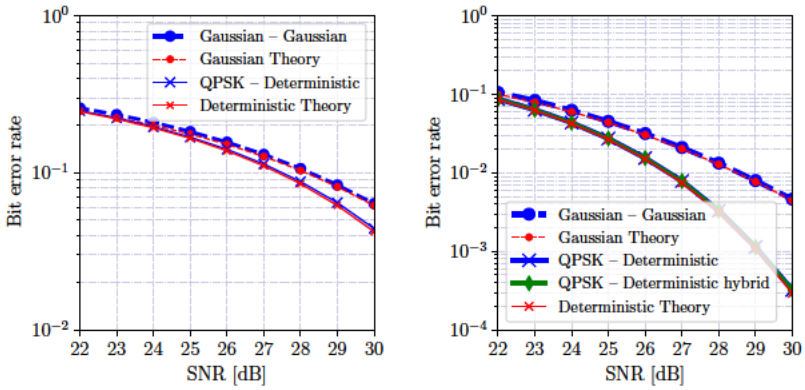

(a) **(b)**

Figure 3.8. Variation in Bit Error Rate (BER) of the optimum receivers for Gaussian ambient signal and for deterministic-unknown ambient signal as a function of mean ambient signal SNR γ when the beamformers are perfectly known for a number of receiver antennas $N_r = 4$ and oversampling rate $K = 4$. In (a), the BD performs OOK, and in (b), BPSK.

3.4 Multi-Antenna BD Modulator Design

Till now, we consider only one ambient source illuminating a single-antenna BD in an AmBC system. In practice, it is likely that signals coming from multiple ambient sources will be impinging on BD. Multiple ambient sources potentially benefit AmBC systems by providing higher signal power that can be harvested and backscattered, which boosts the effective SNR of the BD signal. This section presents that a multi-antenna BD makes effective use of multiple ambient sources, and the derived BD signaling matrices improve the AmBC performance, which is summarized from Publication VI.

3.4.1 Optimum BD Signaling Matrix

The AmBC system is extended to be with N_t single-antenna ambient sources (TX), an N_b-antenna BD, and an N_r-antenna RX. Let $\boldsymbol{H}_d$, $\boldsymbol{H}_r$ and $\boldsymbol{H}_t$ denote the normalized channel matrices of TX–RX, BD–RX and TX–BD, respectively. They are extended from the channels defined in 2.3.1. Let $\boldsymbol{s} \in \mathbb{C}^{N_t \times 1}$ be the vector of the temporal signal transmitted from the ambient sources.

For optimizing the BD signaling matrix, an objective function is obtained by deriving the error probability based on the MAP criterion. The channel matrices and the ambient signal firstly are assumed as being known. The

MAP criterion gives the probability of error as $p_e = \mathcal{Q}(\sqrt{\Delta/2}\|\boldsymbol{H}_r(\boldsymbol{X}_0 - \boldsymbol{X}_1)\boldsymbol{H}_t\boldsymbol{s}\|)$, where Δ denotes the power ratio of the backscatter signal to the ambient signal and $\mathcal{Q}(\cdot)$ denotes the Q-function [96, Chapter 3]. Since the Q-function is monotonic decreasing, p_e is minimized by maximizing the L2-norm $\|\boldsymbol{H}_r(\boldsymbol{X}_0 - \boldsymbol{X}_1)\boldsymbol{H}_t\boldsymbol{s}\|$. The L2-norm indicates the distance between the two modulation states of the backscattered path signal. This yields the optimization problem for obtaining the BD signaling matrix

$$\begin{aligned} \underset{\boldsymbol{X}_0,\boldsymbol{X}_1}{\text{maximize}} \quad & \|\boldsymbol{H}_r(\boldsymbol{X}_0 - \boldsymbol{X}_1)\boldsymbol{H}_t\boldsymbol{s}\|^2 \\ \text{subject to} \quad & 0 \le \|[\boldsymbol{X}_i]_j\|^2 \le 1,\ i = 0, 1,\ j = 1, \cdots, N_b, \end{aligned} \tag{3.24}$$

where the constraint on $\boldsymbol{X}$ is defined in Eq. (2.2).

The global optima of problem (3.24) depends on the ambient signal $\boldsymbol{s}$. When $\boldsymbol{s}$ is known, the optimum $\boldsymbol{X}_0 - \boldsymbol{X}_1$ is chosen so that $\boldsymbol{s}$ is the eigenvector associated with the largest eigenvalue of matrix $\boldsymbol{H}_r(\boldsymbol{X}_0 - \boldsymbol{X}_1)\boldsymbol{H}_t$. However, this requirement is challenging in AmBC systems for two reasons. One is that the AmBC receiver is agnostic about the ambient signal $\boldsymbol{s}$ due to the independence between the legacy system and the AmBC system. The other is that even when $\boldsymbol{s}$ is known, it is unlikely to change the optimal solution of $\boldsymbol{X}$ with every single realization of the fast-varying $\boldsymbol{s}$.

A relaxation is applied to tackle the above challenges. The objective function in problem (3.24) satisfies the inequality

$$\begin{aligned} \|\boldsymbol{H}_r(\boldsymbol{X}_0 - \boldsymbol{X}_1)\boldsymbol{H}_t\boldsymbol{s}\|^2 &\le \|\!|\boldsymbol{H}_r(\boldsymbol{X}_0 - \boldsymbol{X}_1)\boldsymbol{H}_t\|\!|_2^2\|\boldsymbol{s}\|^2 \\ &\le \|\!|\boldsymbol{H}_r(\boldsymbol{X}_0 - \boldsymbol{X}_1)\boldsymbol{H}_t\|\!|_F^2\|\boldsymbol{s}\|^2. \end{aligned} \tag{3.25}$$

Since $\|\boldsymbol{s}\|^2$ is the total transmit power from N_t ambient sources, which is a deterministic and unknown scalar and is independent of $\boldsymbol{X}_i$, the objective function can be heuristically relaxed to its upper bound, i.e., the Frobenius norm. Similarly, the constraint for $\boldsymbol{X}$ is also relaxed to $\|\!|\boldsymbol{X}|\!\|_F^2 = \sum_{j=1}^{N_b} \|[\boldsymbol{X}]_j\|^2 \le N_b$. As a result, the relaxed optimization is given by

$$\begin{aligned} \underset{\boldsymbol{X}_0,\boldsymbol{X}_1}{\text{maximize}} \quad & \|\!|\boldsymbol{H}_r(\boldsymbol{X}_0 - \boldsymbol{X}_1)\boldsymbol{H}_t\|\!|_F^2 \\ \text{subject to} \quad & 0 \le \|\!|\boldsymbol{X}_i|\!\|_F^2 \le N_b,\ i = 0, 1. \end{aligned} \tag{3.26}$$

The relaxed objective function is equal to the square of the expected distance between the two modulation states of backscatter signal that averages over the i.i.d. ambient signal. This implies that the relaxed objective function extricates minimizing p_e from relying on temporal samples of $\boldsymbol{s}$, but in an expected sense.

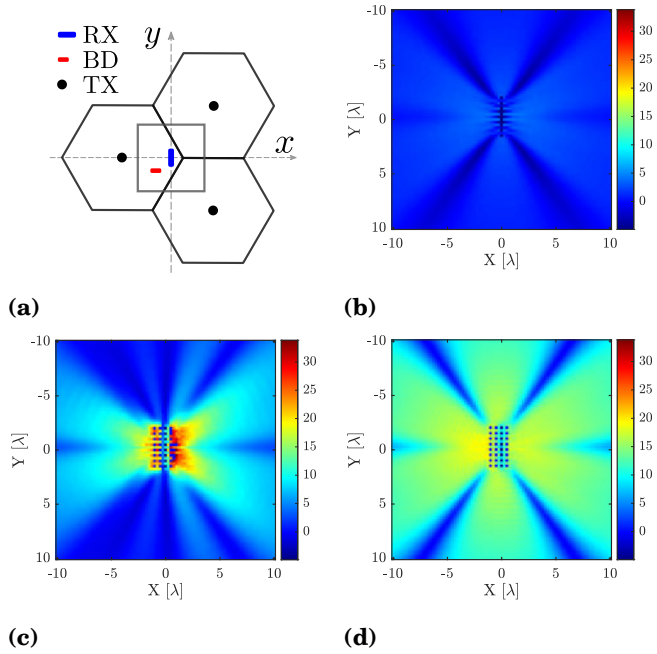

Figure 3.9. The BER performance gain of using multiple antennas at the BD and/or different BD signaling matrix under multiple ambient sources compared to using single antenna at the BD and a single ambient source. In (a), a practical scenario where the grey square marks the area of interest for performance evaluation. The BER ratio in dB of (b) $N_t = 3, N_b = 1$, (c) $N_t = 3, N_b = 4, \boldsymbol{X} = \boldsymbol{I}$, and (d) $N_t = 3, N_b = 4, \boldsymbol{X} = \boldsymbol{X}^\star$ to $N_t = N_b = 1$.

Given the optimization problem, the derived full BD signaling matrix and diagonal BD signaling matrix are respectively expressed as

$$\boldsymbol{X}^\star = \boldsymbol{X}_0 = -\boldsymbol{X}_1 = (1/\|[\boldsymbol{U}_t]_1\|_\infty)[\boldsymbol{V}_r]_1[\boldsymbol{U}_t]_1^H, \tag{3.27a}$$

$$\boldsymbol{X}' = \boldsymbol{X}_0 = -\boldsymbol{X}_1 = (1/\|[\boldsymbol{V}_R]_1\|_\infty)\,\mathrm{diag}([\boldsymbol{V}_R]_1), \tag{3.27b}$$

where the column vectors of $\boldsymbol{U}_m$ and $\boldsymbol{V}_m, m \in \{r, t, R\}$ are the left- and right-singular vectors of matrices $\boldsymbol{H}_r$, $\boldsymbol{H}_t$, and $\boldsymbol{R} = \boldsymbol{H}_t^T \odot \boldsymbol{H}_r$, $\odot$ denotes the Khatri-Rao product, $[\cdot]_1$ takes the 1-st column vector of the matrix, and $\mathrm{diag}(\boldsymbol{a})$ denotes a diagonal matrix with entries $\boldsymbol{a}$. The coefficients $1/\|[\boldsymbol{U}_t]_1\|_\infty$ and $1/\|[\boldsymbol{V}_R]_1\|_\infty$ are multiplied to satisfy the power constraint of the BD signaling matrix expressed in Eq. (2.2). It is evident that the obtained $\boldsymbol{X}$ are beamforming matrices steering the backscatter signal in the direction of the strongest signal strength.

3.4.2 Performance Evaluation

A square area with 20λ length of sides centered around the RX array is considered, as shown in Figure 3.9a. The BER performance of the

single-antenna BD only illuminated by the closest single-antenna TX is selected as the benchmark. Figure 3.9 shows the BER performance gain of using single or multiple antennas at the BD and of using different BD signaling matrices compared to the benchmark. Using the identity signaling matrix, $\boldsymbol{X} = \boldsymbol{I}$, brings a significant performance gain when the BD is extremely close to the RX, i.e., less than 3λ. The gain decays fast as the distance between the BD and the RX increases. Using the optimum signaling matrix $\boldsymbol{X}^\star$ improves the BER performance robustly in the selected area, i.e., roughly a 15 dB gain. As a result, a single-antenna BD cannot effectively uses multiple ambient sources, shown in Figure 3.9b. The identity signaling matrix provides a better BER performance under certain channel conditions while the derived BD signaling matrix largely improves the coverage of AmBC communication.

3.5 Discussion

In this chapter, the designs of the multi-antenna AmBC receivers and the BD signaling matrix subject to minimizing the probability of error are presented. Configuring multi-antenna arrays on AmBC receivers solves the challenges of BD signal demodulation pointed in Section 2.4.1 without relying on specific AmBC setups. This is built upon the spatial selectivity of multi-antenna arrays. By using multi-antenna arrays to find the strongest signal direction when the BD does not operate, DPI is canceled by projecting the received signal into its null space, and the unknown ambient signal can be coarsely estimated. Configuring multiple antennas on BDs improves the AmBC communication range, especially when there are multiple ambient sources.

These designs all explore the channels altered by BD transmissions. The coherent receiver examines the phase offset caused by the excess path length of the backscatter path channel while the optimum receivers consider the composite channel. The receiver performance analyses show that the key parameters affecting the coherent receiver and the optimum receivers are Δ_e and κ, respectively. The former indicates the effective SNR of the backscatter signal after the DPI has been nullified. The latter evaluates the direction variation between the composite channel under two BD modulation states, which indirectly indicates the effective SNR of the backscatter signal. Both imply the alternation caused by BD transmission and also show the separability of the two modulation states of the

BD signal. The two parameters also suggest that placing the BD at an appropriate location increases the alternation.

Even though the phase offset caused by the excess path length of the backscatter signal cannot be directly estimated, the research in this thesis proposes an ML-assisted method to learn the pattern of the phase offset and set the decision boundary. This equivalently accomplishes the phase-coherent operation. Non-coherent receivers, due to the phase ambiguity, in general, require a higher SNR compared to coherent receivers. However, the non-coherent optimum AmBC receiver achieves the same performance as the coherent receiver, where the performance comparison is shown in Figure 3.4b. The reason is stated as follows. The BD signals affect the received signal by changing the composite channel so that they can be taken into account as a whole when deriving the likelihood functions. Since the channels assume block-fading, the conditional density of $\boldsymbol{y}$ for a given BD symbol x can be equivalently written conditioning on $\boldsymbol{g}$, i.e., $f(\boldsymbol{y}|x = x_0) \equiv f(\boldsymbol{y}|\boldsymbol{g} = \boldsymbol{g}_0)$, and $f(\boldsymbol{y}|x = x_1) \equiv f(\boldsymbol{y}|\boldsymbol{g} = \boldsymbol{g}_1)$. This also implies that once the composite channel is obtained, the unknown phase offset and the phase of the channels are constant within the frame transmission. The derived likelihoods do not depend on the phase, and thus, there is no SNR penalty due to phase ambiguity. Hence, the receiver is non-coherent in nature requiring no phase-coherent operation, and yet it achieves the performance of the coherent receiver.

The equivalence of the optimum receivers for two different types of ambient signal, summarized in Section 3.3, is shown under certain circumstances. One condition holding for nearly all practical AmBC deployments is that the channel gain difference between the direct path and the backscatter path should be large. The other one with a high total received SNR of the ambient signal is also related to the deployment of AmBC systems. This indicates that successful transmission of AmBC systems requires a good ambient signal condition. This equivalence extends the optimum receiver presented in [23] by showing that a Gaussian ambient signal is not required for most of the practical scenarios. Therefore, the receivers support general binary-modulated BD signals and different types of ambient signal. Furthermore, unlike AmBC receivers in the literature and the coherent receiver, the resultant optimum receiver requires neither a complicated DPI cancellation nor phase synchronization. As shown in [23], it also avoids the error floor problem. As such, the optimum receiver provides a better AmBC system performance enhancement compared to

state-of-the-art methods.

For multi-antenna BDs, the reflection coefficients are tuned to maximize the difference of the alternation caused by BD transmission between the two modulation states. It is shown that using the optimum BD signaling matrix on a multi-antenna BD is an attractive solution when there are multiple ambient sources. It increases the BD communication range compared to the often applied identity signaling matrix. The derived BD signaling matrix requires BD modulators with infinite resolutions (change the phase and amplitude to arbitrary value). This yields BDs with high manufacturing costs. It is shown in Chapter 4 that discretizing BD signaling matrices properly approaches the performance of continuous ones.

The channel gains of the direct path and backscatter path do not discriminate between different fading processes as long as their individual components experience a single realization of the channel gain within one BD frame duration. The small-scale fading changes the observed SNR of both ambient and backscatter signals and might yield poor receiver performance. Therefore, the mere impact of small-scale fading losses is to shift the BER performance curves slightly toward higher SNR values, which can be compensated by increasing the number of samples acquired for each BD symbol K, or applying coding schemes. Therefore, the derived receivers can handle small-scale fading effects without a need for special treatment in the receiver architecture.

The above assumption fails when one or more system nodes are mobile, or when, as is a frequent case, the ambient system is wideband. In a time-selective channel condition, a multi-antenna non-coherent AmBC receiver that averages over the varying channels is studied in [72], and the use of Manchester coding to combat time-selectivity is proposed in [102]. Considering a wideband ambient signal, the work [52] proposes to interleave the BD preambles and BD data symbols as well as use a spreading code to obtain a better estimate of channel statistics. In order to implement the proposed AmBC receivers when the ambient signal is a wideband signal, a processing method that extracts the signal in the narrowband is summarized in Section 4.3.

The projected BD ranges are larger than the reported ranges for different AmBC implementations. For an AmBC system using the TV signal as an ambient source [11], the transmission distance between a passive BD and RX is up to 1 meter (1.5λ) when the TV tower (TX) is more than 4 kilometers away from BD and RX. In [103], the BD achieves successful

communication when the distance between the BD and RX is 50 meters and the distance between the TX and BD is fixed to be 1 meter (4λ) for the 802.11b ambient signal. The communication range for a long-range (LoRa) ambient signal can reach up to 1.1 kilometers between the BD and RX when the BD is placed 0.2 meters (less than a λ) away from the TX [104]. The projected ranges can be drastically improved by using time diversity, e.g., by increasing the oversampling rate K or using coding, and/or by using multi-antenna BDs. Therefore, the designs summarized in this chapter are expected to improve the AmBC system range significantly.

4. Practical Implementation and Measurements

The designs presented in the previous chapter minimize the probability of error for demodulating a BD signal. All derivations are accounted under certain assumptions. Successful implementation of these designs requires specific considerations on these assumptions. In this chapter, we focus on the implementation of the designs to improve their practicality. The first two sections discuss key challenges regarding implementing AmBC receivers and multi-antenna BD signaling matrices. Section 4.3 presents an experiment of an AmBC system for validating the derived multi-antenna receivers.

4.1 Receiver Implementation

For the optimum receiver, the test statistics for a deterministic-unknown ambient signal and for a Gaussian-distributed ambient signal are z_d in Eq. (3.18) and z_g in Eq. (3.19), respectively. Both z_d and z_g are the difference of the quadratic functions of measurement $\boldsymbol{y}$. Let $\boldsymbol{G}(x_i)$ denote either $\boldsymbol{G}_g(x_i)$ or $\boldsymbol{G}_d(x_i)$, the two test statistics can be written in a general form as

$$\begin{aligned} z =& \sum_{k=1}^{K} \left(\boldsymbol{y}^H[k] \boldsymbol{G}(x_1) \boldsymbol{y}[k] - \boldsymbol{y}^H[k] \boldsymbol{G}(x_0) \boldsymbol{y}[k] \right) \\ =& \sum_{k=1}^{K} \|\boldsymbol{B}^H(x_1) \boldsymbol{y}[k]\|^2 - \sum_{k=1}^{K} \|\boldsymbol{B}^H(x_0) \boldsymbol{y}[k]\|^2, \end{aligned} \tag{4.1}$$

where $\boldsymbol{B}(x_i)$ satisfying $\boldsymbol{G}(x_i) = \boldsymbol{B}(x_i)\boldsymbol{B}^H(x_i)$ is referred to as the *beamforming matrix*. For the two cases of the ambient signal, the beamforming matrices are given by

$$\begin{aligned} \boldsymbol{B}_d(x_i) &= \boldsymbol{G}_d^{\frac{1}{2}}(x_i) = \boldsymbol{I} - \frac{\boldsymbol{g}_i \boldsymbol{g}_i^H}{\|\boldsymbol{g}_i\|^2}, \\ \boldsymbol{B}_g(x_i) &= \boldsymbol{G}_g^{\frac{1}{2}}(x_i) = \boldsymbol{I} - (1 - \frac{1}{\sqrt{1 + \sigma_s^2 \|\boldsymbol{g}_i\|^2}}) \frac{\boldsymbol{g}_i \boldsymbol{g}_i^H}{\|\boldsymbol{g}_i\|^2}. \end{aligned} \tag{4.2}$$

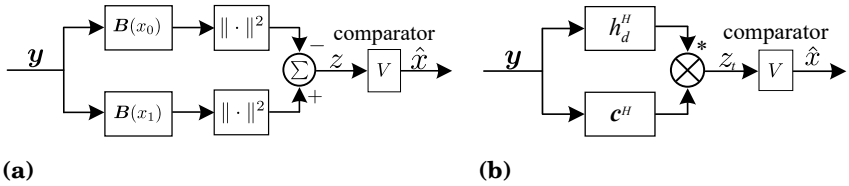

Figure 4.1. Implementations of (a) the optimum receiver with two beamforming matrices and (b) the ML-assisted coherent receiver.

A receiver that makes a decision using the test statistic in Eq. (4.1) can be implemented as a square-sum device after beamforming $\boldsymbol{y}$ using $\boldsymbol{B}(x_i)$, as illustrated in Figure 4.1a. The received signal is split into two streams to feed two branches. Each of the streams goes through a beamforming matrix, and through a square-sum device to calculate the norm-squares of the beamforming output. The receiver makes a decision by comparing the difference of the norm-square with the decision threshold V.

For the ML-assisted coherent receiver, the test statistic z_t in Eq. (3.11) is a multiplication of two beamformed outputs with directions $\boldsymbol{h}_d$ and $\boldsymbol{c}$. An implementation of this receiver is shown in Figure 4.1b. The received signal is split into two branches. Each of the branches goes through an inner product processor. The outputs are multiplied yielding the test statistic which is then compared to the decision boundary V for inference. The decision boundary is calculated using the LR algorithm when the BD transmits two known BD sequences as shown in Section 3.2.

The beamformer products in the optimum receiver shown in Figure 4.1a at first glance can be implemented as a matrix-vector product processor. However, noticing that the beamformers are the difference between an identity matrix and a rank-one matrix, it also only requires an inner product and a vector difference processor. Thus, their hardware implementation requirements are not higher than standard multi-antenna receivers.

4.1.1 Estimation of Beamformers

The directions $\boldsymbol{h}_d$ and $\boldsymbol{c}$ in z_t, the beamforming matrices $\boldsymbol{B}(x_i)$ in z and the decision threshold V can be calculated from a conditional auto-correlation matrix of the measurements when the BD signal is given. For the optimum receivers, the auto-correlation matrix of $\boldsymbol{y}$ in Eq. (3.14a) conditioned on $x = x_i$ is

$$\boldsymbol{R}_{\boldsymbol{y}|x_i} = \mathrm{E}\{\boldsymbol{y}\boldsymbol{y}^H|x_i\} = P_s\boldsymbol{g}_i\boldsymbol{g}_i^H + \boldsymbol{I}, \tag{4.3}$$

where $P_s = |s|^2$ for a deterministic-unknown ambient signal and $P_s = \sigma_s^2$ for a Gaussian-distributed ambient signal. Its largest eigenvalue $1 + P_s\|\boldsymbol{g}_i\|^2$ and the associated eigenvector $\boldsymbol{g}_i/\|\boldsymbol{g}_i\|$ are needed to construct the decision boundary and the test statistics. For the coherent receiver, the two directions are the eigenvectors associated with the largest eigenvalue of the auto-correlation matrices of the received signal $\boldsymbol{y}$ when $x = 0$ and of the residual signal $\boldsymbol{r}$ in Eq. (3.7), respectively. Therefore, for these receivers, an estimate of the corresponding auto-correlation matrix is required. In what follows, we mainly consider the optimum receiver since it is straightforward to extend the implementation discussion to the coherent receiver.

The auto-correlation matrix estimation has well-known solutions. Among the alternatives, the easiest is to collect samples when the BD transmits the preamble sequences. The estimate of the conditional sample auto-correlation matrix converges to a positive definite Hermitian matrix when the length of the preamble L is larger than N_r. Since only the largest eigenvalue and its associated eigenvector are needed, the *power iteration* method [105, Section 8.2.1] is utilized. Let $\hat{\boldsymbol{R}}_{\boldsymbol{y}|x_i}$ be the auto-correlation matrix estimate. The power iteration method reads as

$$\hat{\boldsymbol{u}}^{(\iota+1)} = \frac{\hat{\boldsymbol{R}}_{\boldsymbol{y}|x_i}\hat{\boldsymbol{u}}^{(\iota)}}{\|\hat{\boldsymbol{R}}_{\boldsymbol{y}|x_i}\hat{\boldsymbol{u}}^{(\iota)}\|}, \tag{4.4}$$

for the iteration number $\iota = 0, 1, \cdots$. The calculation stops when the eigenvector estimate $\hat{\boldsymbol{u}}^{(\iota)}$ satisfies a convergence criteria for its associated eigenvalue estimate, given by

$$\hat{\mu}^{(\iota)} = \hat{\boldsymbol{u}}^{(\iota)H}\hat{\boldsymbol{R}}_{\boldsymbol{y}|x_i}\hat{\boldsymbol{u}}^{(\iota)}. \tag{4.5}$$

The algorithm converges if i) the initial vector $\hat{\boldsymbol{u}}^{(0)}$ has a non-zero and significant component along the largest eigenvector, and ii) the largest eigenvalue is unique, and its separation from the closest eigenvalue is high enough with respect to the machine precision.

For the considered problem, the method converges when $|s|^2\|\boldsymbol{g}_i\|^2$ or $\sigma_s^2\|\boldsymbol{g}_i\|^2$ is high and the eigenvector estimate is initialized appropriately. The former requirement is satisfied when the SNR of the ambient signal is high, which is the common case in AmBC systems. In practice, the initial estimate of the eigenvector can be set to an estimate of the direct path channel $\boldsymbol{h}_d$, which can be calculated using the measurements acquired when the BD is not operating. Therefore, power iteration is an appealing method to find the largest eigenvalue and associated eigenvector of the sample auto-correlation matrix to estimate the beamformers.

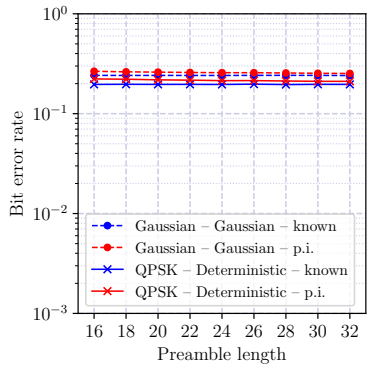

Figure 4.2. Variation in BER as a function of preamble length L when the maximum eigenvalue and the corresponding eigenvector of the sample auto-correlation are perfectly known (known) and when they are estimated using power iteration method (p. i.) for $N_r = 4$ and $\gamma = 24$ dB.

The performance of the receiver depends on the estimation quality of the beamformers. Since the receiver uses the samples received from the BD preamble sequences, the length of the preamble L and the estimation method affect the estimation quality. In Publication III and Publication V, their impacts on BER performance are evaluated. A result shown in Figure 4.2 concerns the optimum receivers for the two types of ambient signal, in which the power iteration method is such that it has maximum 10 iterations for a 10^{-16} tolerance level. When s is Gaussian-distributed, the two Gaussian receiver implementations have a negligible performance difference in the considered parameter ranges. For a QPSK-modulated ambient signal, the implementations have a small BER performance difference, but the difference decreases with increasing preamble length. A preamble length of $L = 32$ in this case provides enough samples for power iteration to estimate the beamformers.

4.1.2 Supported Ambient Systems and Signals

The sample auto-correlation matrix estimate using $\boldsymbol{y}$ in Eq. (3.14a) given a transmitted BD signal can be written as

$$\hat{\boldsymbol{R}}_{\boldsymbol{y}|x_i} = \frac{1}{L}\sum_{l=1}^{L} \boldsymbol{y}[l]\boldsymbol{y}^H[l] \approx \boldsymbol{g}_i\boldsymbol{g}_i \frac{1}{L}\sum_{l=1}^{L} |s[l]|^2 + \boldsymbol{I}, \tag{4.6}$$

where L denotes the preamble length. The approximation is valid when L is large, the measurement noise process $\boldsymbol{n}$ is ergodic in the wide sense, is independent of s and has a zero mean. These are implied by the definition of the measurement noise and the selection of preamble length. The expression also requires the channel gains to be constant, which is valid

for a block-fading channel with coherent time exceeding the BD frame duration. The square sum of the time samples of the ambient signal should be finite to guarantee the convergence of the sum, which indicates that the ambient signal should have a finite power. This requirement is not restrictive for practical ambient source transmitters. Therefore, for all practical ambient systems, the estimation of the auto-correlation matrix in Eq. (4.6) is valid.

For the type of supported ambient signal, let us assume that s is a wide-sense ergodic random process with mean μ_s and variance σ_s^2. Then, the sum in Eq. (4.6) converges to

$$\frac{1}{L}\sum_{l=1}^{L}|s[l]|^2 \rightarrow \sigma_s^2 + |\mu_s|^2. \tag{4.7}$$

The mean $\mu_s = 0$ for all modulation types with signal constellation points symmetrical around the zero of the complex plane[1]. The variance σ_s^2 is defined by the transmitted data sequence, modulation type and the spectral properties of the transmitter filter. For a given transmitter filter and equally probable symbols, the variance can be calculated from the power spectral density of the modulation [81, Section 3.4]. For equally probable FSK and PSK, the variance $\sigma_s^2 = |s|^2$ is equal to the symbol power as all symbols have equal amplitude. For ASK, the variance is equal to the average signal power. The more complex modulations, such as OFDM, have more involved variance expressions, and their signals can be treated as Gaussian variables. Therefore, all ambient signals from symmetrical constellations are supported by the AmBC receiver for a deterministic-unknown s, and ambient signals of more complex modulations are supported by the receiver for a Gaussian-distributed s. Since these two receivers are equivalent when SNR is high, the receiver for deterministic-unknown s supports all types of ambient signals with zero mean.

The derivations assume that the ambient signal is always present. When this assumption fails, the receiver must identify first the presence of s, and then try to decode the BD symbol. This problem has well-known solutions in cognitive radio literature, e.g., the solutions provided by Zhang et al. [106]. For ambient systems that transmit information on a sporadic basis, an AmBC system requires more careful design.

[1]On-off keying has a non-zero mean. However, since in zero state no energy is transmitted, ambient systems using on-off keying modulation are not considered.

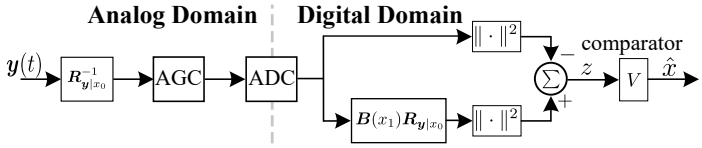

Figure 4.3. An analog-digital hybrid implementation of the optimum receiver with two beamformers, one in analog domain that suppresses the direct path signal before automatic gain control (AGC) operating before ADC.

4.1.3 Dynamic Range Issue

The beamformer estimator requires N_r digital streams, which implies that the receiver can be implemented using N_r number of RF front-ends, each followed by an ADC. The receivers given in Figure 4.1a are example implementations in the digital domain.

In practice, the dynamic range of ADC determines the quality of the numerical representation of the measurements $\boldsymbol{y}$. As the DPI is much stronger than the backscatter signal, the significant bits of the digital value of $\boldsymbol{y}$ represent the direct path signal, while the backscatter signal is limited to the least significant bits. Successful receptions of the BD signal require ADC to have a high dynamic range. One solution to overcome the dynamic range problem is to implement one of the beamformers in the analog domain and the other in the digital domain as shown in Figure 4.3. The BER performance of such an analog-digital hybrid receiver is also shown in Figure 3.8b (see the curve QPSK – Deterministic hybrid). It has the same performance as the fully digital implementation and can be used as a practically advantageous implementation of the optimum receiver. Although this implementation provides practical gains, it requires additional implementation details such as resetting the analog beamformer gains when a frame reception is over. Nonetheless, the receiver shown in Figure 4.3 can handle numerical problems that might occur in a fully digital implementation.

An alternative method that can avoid the dynamic range problem for the optimum receiver is studied in Publication IV. A *simplified receiver* is derived through disposing of one branch of the optimum receiver and only considering the measurement that falls in the subspace of the kept beamforming matrix. As shown in Figure. 4.4a, the simplified receivers for a deterministic-unknown ambient signal and for a Gaussian-distributed ambient signal take the same structure which is written as

$$z_s \triangleq |\boldsymbol{b}^H \boldsymbol{y}|^2 \underset{\mathcal{H}_1}{\overset{\mathcal{H}_0}{\gtrless}} V. \tag{4.8}$$

The beamformer

$$\boldsymbol{b} = \frac{\boldsymbol{G}_0\boldsymbol{g}_1}{\|\boldsymbol{G}_0\boldsymbol{g}_1\|} = \frac{(\boldsymbol{I} - \boldsymbol{g}_0\boldsymbol{g}_0^H/\|\boldsymbol{g}_0\|^2)\boldsymbol{g}_1}{\|(\boldsymbol{I} - \boldsymbol{g}_0\boldsymbol{g}_0^H/\|\boldsymbol{g}_0\|^2)\boldsymbol{g}_1\|} \tag{4.9}$$

is the same, but the threshold V varies with the signal type. Since the beamformer can be implemented fully in the analog domain, the dynamic range problem can be mitigated. Compared with the optimum receiver, the number of RF front-ends necessary to implement the receiver can be halved. This, nevertheless, suffers from a modest SNR penalty of 1-dB to achieve the same performance as the optimum receiver for the deterministic-unknown ambient signal and of 3.6-dB for the Gaussian-distributed ambient signal, as can be seen from the BER performance comparison in Figure 4.4b. Therefore, the simplified receiver is a cost-efficient solution of mitigating the dynamic range issue although it has a performance degradation.

The derived simplified receiver is equivalent to the zero-forming (ZF)-based receiver proposed in [19]. Compared to [19], we thoroughly derive the receiver test statistic based on the MAP criterion, we further analyze the receiver performance. The ZF-based receiver implies that the beamformer nulls one signal direction but considers the component of $\boldsymbol{g}_1$ that is orthogonal to $\boldsymbol{g}_0$. Hence, the receiver relies heavily on the separability of two directions, and assumes the signal comes from one main unresolvable direction. In the case of an OOK-modulated BD signal, the BD should be placed in the location away from the line between the TX and the RX array. Additionally, the simplified receiver suffers performance degradation since it does not consider the noise when calculating the beamformer.

4.2 Multi-Antenna BD Implementation

4.2.1 Estimation of BD Signaling Matrix

One critical challenge about the multi-antenna BD presented in Section 3.4 is the acquisition of the BD signaling matrix. Since the BD per se is a passive device, its operations are restricted by the limited amount of energy. In this regard, several approaches of obtaining the signaling matrix for a BD are discussed.

One approach is to resort to the AmBC receiver which estimates the BD signaling matrix and then feeds that estimation to the BD. Even though the BD needs a receiver, the receiver of a feedback channel is

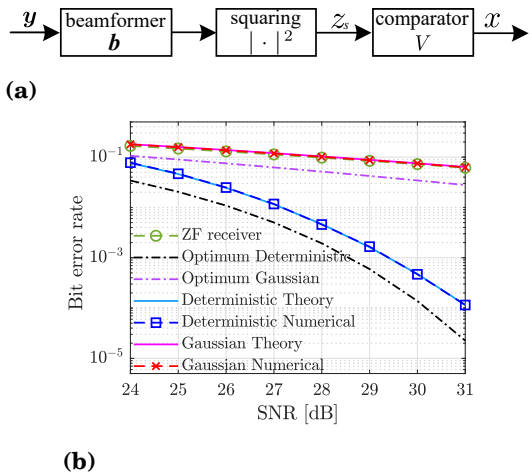

Figure 4.4. In (a), implementation of the simplified receiver. In (b), comparison of BER as a function of ambient signal SNR γ for $N_r = 16$ between the numerical BER of the ZF-based receiver in [19], the probability of error of the optimum receiver of the two types of ambient signal in Publication V, and the probability of error and numerical BER of the simplified receiver for the two types of ambient signal.

not power demanding, and the passive receiver presented in [33] can be readily adopted. Nevertheless, the right- and left-singular vectors that form the optimal signaling matrix in Eq. (3.27) cannot be extracted from the cascaded backscatter channel. To tackle this challenge, an estimation scheme that requires the BD to send specific training sequences is proposed in Publication VI.

Estimating the full and the diagonal signaling matrices requires $N_b^2 + 1$ and $N_b + 1$ preamble sequences within one BD frame, respectively. During the preamble sequences, initially the BD stays silent and then wakes up a single modulator while keeping others silent. The receiver estimates the channel coefficients associated with each preamble sequence. The BD signaling matrices are obtained from the singular vector decomposition of these channel estimates. The channel estimation can be done by using, for example, the maximum likelihood estimator which requires the information of the ambient signal. Obtaining the ambient signal can be realized by attaching a standard ambient signal receiver to the AmBC receiver. The performance of the estimation method is evaluated as a function of the length of training sequence L. It is shown in Publication VI that the estimation for the diagonal BD signaling matrix converges slower than that for the full BD signaling matrix. In addition, the estimation method provide an acceptable performance when $L \geq 100$.

The above method is feasible when all the ambient sources belong to

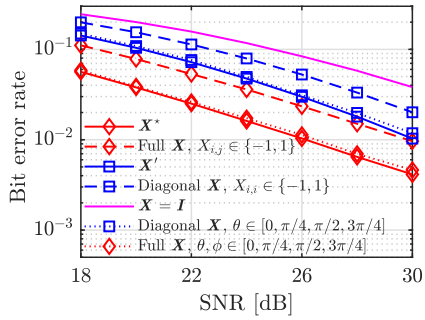

Figure 4.5. BER comparison between the optimal signaling matrix and that selected from discretized sets.

the same type, such as when the ambient sources are multiple DVB-T base stations. However, it is challenging for the AmBC receiver to acquire information about different types of ambient sources. To lift the constraint of knowing the ambient signal, one can configure the BD with an RF chain [107]. The BD then estimates the signal direction associated with the strongest signal power towards the TX. The beamformer toward the RX can be acquired from the RX using channel reciprocity. Such an implementation can be realized using the beam-steerable transponder [108] and an energy detector at the BD.

4.2.2 Discretized Signaling Matrix Set

A pre-defined discretized signaling matrix set facilitates the selection of the BD signaling matrix by evading complicated channel estimation. BDs can, for example, select the best BD signaling matrix from the pre-defined set by brute-force searching, and use it for a BD frame duration. A set with smaller cardinality lessens the BD power consumption because it decreases the required bits for the AmBC RX to feedback the optimum BD signaling matrix. The sets that can be formulated are decided by the resolution of each BD modulator. Lowering the resolution of each modulator can reduce the BD manufacturing cost. The resolution, on the other hand, decides the performance of the BD signaling matrix.

A straightforward set contains 1-bit BD modulators, that is, $[X]_{i,j} \in \{-1, +1\}$. Considering that the optimum signaling matrix is a beamforming matrix, another discrete set is quantized beamforming angles and the signaling matrices are formed by the steering vectors. For example, let us consider the full signaling matrix $\boldsymbol{X} = \boldsymbol{\alpha}(\theta_1)\boldsymbol{\alpha}(\theta_2)^H$ and the diagonal signaling matrix $\boldsymbol{X} = \mathrm{diag}(\boldsymbol{\alpha}(\theta_2))$ where $\theta_1, \theta_2 \in \{0, \pi/4, \pi/2, 3\pi/4\}$, and

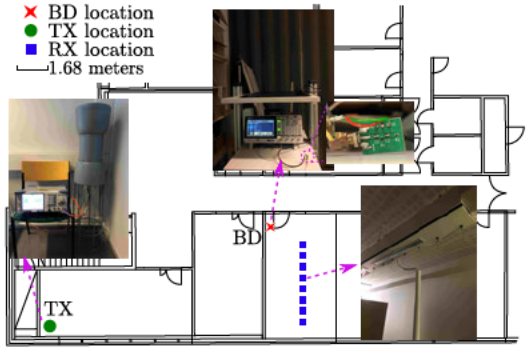

Figure 4.6. The measurement scene of the AmBC system.

the k-th element of the steering vector $[\alpha(\theta)]_k = \exp(-j\pi\cos\theta(k-1))$. The cardinalities of the two sets are 2^{16} and 16, respectively, while the latter requires a higher resolution. The comparison of BER performance is shown in Figure 4.5. As can be seen, with properly quantized beamformers, the BD signaling matrix outperforms the 1-bit modulator and approaches the derived BD signaling matrix with continuous resolution.

4.3 Receiver Experiment

In this section, the multi-antenna AmBC receivers proposed in Publication V, Publication IV and [19] are implemented using low-cost COTS antennas and software-defined radios (SDRs) with a small form factor. Unlike the derivations in the last chapter where the ambient signal is assumed to be narrowband, the measurement takes a wideband signal which is used in most current wireless systems[2]. Practical issues in regard to low-cost implementation are identified. A signal processing method is proposed for a successful implementation. The content is summarized from Publication VII.

4.3.1 Measurement Setup

A measurement scene of an AmBC system is set up as shown in Figure 4.6, and the configuration parameters are given in Table 4.1. Let the RX antenna that is closest to the BD be the 1-st antenna. This gives the distances $d_{0,1} \approx 22.7\lambda$, $d_{1,1} \approx 3.9\lambda$ and $d_2 \approx 23.3\lambda$. The measurement is carried out in a rich-scattering indoor environment such that the path-loss

[2]Wideband indicates that the bandwidth of a signal exceeds its coherence bandwidth.

Table 4.1. Measurement setup parameters

	Parameter	Value
TX	Baseband signal generator	R&S SMBV100A Vector Signal Generator
	Antenna	R&S HK033 VHF/UHF coaxial dipole
	Carrier frequency	483 MHz
	Bandwidth	8 MHz
	TX power level	6, 8, 10, 12, 14 dBm
	Signal type	OFDM signal with a reference subcarrier and random information subcarriers
BD	Baseband signal generator	Tektronix AFG 31000 Arbitrary Function Generator
	Antenna	Nooelec M6 antenna
	Modulation loss	$\leq$ 1dB
	Modulation scheme	OOK
	Modulation rate	100 kilobits-per-second
RX	Device	XTRX
	Antenna	Nooelec 433 MHz ISM antenna mast
	Analog-to-digital converter	12 bits
	Number of antennas	8
	Sampling rate	10 MHz
	Low noise amplifier	26 dB
	Programmable gain amplifier	2 dB

exponent is higher than 2, which gives rise to a larger-than-34-dB power difference between the backscatter path signal and the direct path signal.

TX end

The ambient signal is an OFDM signal that comprises one reference subcarrier and random information subcarriers. The reference subcarrier has a 3-dB higher SNR compared to the information subcarriers. The carrier frequency of the ambient signal is 483 MHz with a bandwidth of 8 MHz. The ambient signal generated using MATLAB is input into a Rohde&Schwarz (R&S) SMBV 100A signal generator and then transmitted by an R&S HK033 omnidirectional antenna.

BD end

The BD is driven by an arbitrary function generator to send its baseband signal which is generated using MATLAB. Since the RX requires the BD

preambles for estimating the test statistics of the receivers during one channel coherence time, one BD frame starts with the first two $L = 50$ sequences as preambles, followed by 900 BD information symbols. The information symbols are drawn from the binary uniform distribution, i.e., $\Pr(x_0) = \Pr(x_1) = 0.5$. The BD frame is then fed into a signal generator to generate the waveform which is transmitted through a COTS antenna.

AmBC receivers rely on the condition that channels stay constant for the duration of interest. Hence, the BD frame duration should be equal to or less than the channel coherence time. When the channel varies, preamble sequences need to be sent for sounding the environment and for computing test statistics and decision thresholds. In addition, a preferred BD data rate depends on the target application. These jointly determine BD symbol duration and BD frame length. Hence, a BD frame can be finely tuned for achieving a desired throughput of an AmBC system. In the measurement, the BD data rate is set to be 100 kilobits-per-second considering the channel coherence time in an indoor office environment with the utilized carrier frequency.

RX end

The RX acquires in-phase/quadrature (I/Q) data using four XTRX boards that connect to a PC through PCI express. The XTRX is a type of SDR board, which has two channels that are connected to the antennas placed on the office ceiling. The four boards share the same parameters, including local oscillator frequency, sampling frequency, and low noise amplifier gain which can be customized on the PC.

As discussed earlier in the thesis, due to the keyhole channel effect, the backscatter signal strength is extremely weaker than the direct path signal. The backscatter path signal is buried in the least significant bits. The successful reception of the weak signal imposes a higher requirement on the ADC to have a large dynamic range. Even though two solutions are provided in Section 4.1.3, they take the analog domain into consideration. This experiment considers the digital implementation. The XTRX has a 12-bit ADC. In addition, the gains of the low noise amplifier and the programmable gain amplifier can be tuned to improve the ADC dynamic range. Low noise amplifier, a building block at the XTRX front end, helps boost the received signal to be higher than the noise floor, especially for the weak backscatter signal. In our setup, in order to observe the complete backscatter signal, the low noise amplifier gain is set to 26 dB. Adding a

programmable gain amplifier increases the dynamic range of the circuit by increasing the resolution per bit. The programmable gain amplifier value is set to 2 dB.

The measurement has downplayed the synchronization between the BD and the AmBC receiver since the measurement mainly concerns the proof-of-concept implementation of the multi-antenna AmBC receivers and their performance evaluation. The synchronization is realized by using a second signal generator which sends a trigger signal to the RX via coaxial cable when the BD starts to transmit the baseband signal. Nevertheless, the initial acquisition of the backscatter signal is of great significance and needs to be carefully investigated for practical AmBC systems.

4.3.2 Processing

Limitations on direct implementation

The multi-antenna AmBC receivers exploit the directionality of the signal which is done via beamforming on a multi-antenna array. This relies heavily on the behavior of each channel, including the wireless propagation channel and the channel from the antenna to the I/Q demodulator, such that the phase rotations among all the channels are relatively the same. In the previous chapter, the AmBC receivers are investigated under certain specific assumptions. These assumptions are that the system is narrowband and the RF front-ends on the transceivers are ideal. They make the requirement that the phase rotations are relatively the same within one channel coherence time fulfilled. However, there usually are some situations in practical implementations where these assumptions are not satisfied. The channel behavior can be unstable. One reason is the utilization of COTS antennas and small-form-factor SDRs. COTS products are susceptible to hardware impairments since they can be unstable and uncontrollable even though they facilitate cost-efficient AmBC receiver implementations. Another reason is due to the wideband ambient systems. In a narrowband system, the frequency responses of antenna elements are constant in the frequency band of interest. When it comes to a wideband system, the frequency responses vary differently among antenna elements. Each antenna has a different time-varying gain, which degrades the beamforming performance. Such a phenomenon is known as the *wideband effect* [109].

In a system with unstable RF front-ends and wide bandwidth, the re-

ceived signal is distorted by, such as signal interference, channel congestion, and noises. These disturbances significantly decrease the observed SINR of the backscatter signal. Moreover, there is no synchronization between the ambient TX and the AmBC RX, and different XTRX channels may have asynchronous ADC local oscillator frequencies. The receiver test statistics calculated during the preamble time cannot capture the time variations, which degrades the beamforming performance. Therefore, in these situations, the AmBC receivers cannot be applied directly.

Processing method

In order to implement the low-cost multi-antenna AmBC receivers under a practical wideband ambient system, a processing method is proposed in Publication VII. The method makes use of reference signals of ambient systems that are transmitted for the purpose of control signaling. Considering OFDM systems, reference signals occupy specific narrowband subcarriers, whose frequency allocations are easily available for AmBC systems. Given these frequency allocations, AmBC receivers can extract the received signal in the reference subcarriers. Hence, the varying frequency response of antenna elements over the wideband is avoided.

The AmBC receiver acquires the I/Q samples and processes the samples offline. The processing procedure is shown in Figure 4.7. The AmBC receiver first shifts the reference signal to the baseband and applies a low-pass filter to obtain the reference subcarrier signal. Within the passband, there remains interference including inter-symbol interference and inter-carrier interference. Then, to remove the remaining interference, the principle component analysis (PCA) is used to denoise the signal. The PCA separates the passband further into frequency bins and selects the dominant bin that mainly contains the reference signal. After the denoise, the test statistic and decision threshold of a receiver are computed from the training sequences, as described in Section 4.1.1. However, the test statistics exhibit a curvilinear trend with low frequency caused by time-varying components falling inside the selected bin. As such, a high-pass filter is applied to remove the trend. Finally, the BD signal can be demodulated by comparing the processed test statistic with the decision threshold.

4.3.3 Measurement Results

The BER performance of the BD signal using several AmBC receivers is presented in Figure 4.8. We observe that the simplified receiver has a bad

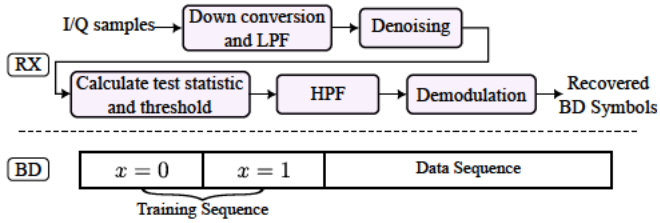

Figure 4.7. An illustration of the BD frame and the flowchart of RX processing procedure where LPF denotes low-pass filter and HPF denotes high-pass filter.

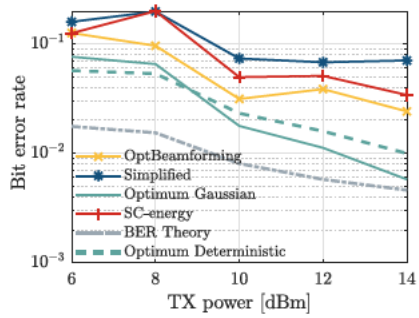

Figure 4.8. Variations in BER as a function of TX transmit power in dBm for different multi-antenna AmBC receivers: Optimum Gaussian and Optimum Deterministic from Publication V, Simplified from Publication IV, and OptBeamforming and SC-energy studied in [19].

performance. The reason is that the received signal contains many resolvable directions. The selective combining (SC)-based energy receiver obtains the diversity gain and outperforms the simplified receiver. The optimum receivers outperform the others. In addition, because the difference between g_0 and g_1 is small in the measurement set, the two types of the optimum receiver are not equivalent. Among the two optimum receivers, the optimum deterministic has slightly better performance in the low transmit power region because the ambient signal is deterministic unknown. As the transmit power increases, the optimum Gaussian performs better. This is due to the multipath effect in wideband systems. The multipath components become stronger as transmit power increases. The optimum Gaussian receiver takes the multipath components into consideration while the optimum deterministic only considers the strongest direction. The probability of error of the optimum receiver for the deterministic-unknown ambient signal is calculated using the result from Section 3.3.2. Compared to the probability of error, the measurement result can achieve the same BER with roughly 4 dB higher transmit power. This gap may come from the phase noise induced by the unstable RX front-ends.

4.4 Discussion

In this chapter, practical implementation issues regarding the designs of the multi-antenna AmBC receivers and the BD signaling matrix are discussed and solutions are provided for the identified problems. The simulation results show that the proposed estimation method for parameters constructing the designs is valid and provide accurate estimates. The methods for receiver designs do not require information on the ambient signal. However, estimating the BD signaling matrix at AmBC receivers requires a known ambient signal. This restricts the AmBC system to have cooperative ambient systems, or to be able to demodulate the ambient signal. To relax this restriction, two alternatives are proposed. In particular, using a discretized set of BD signaling matrices has practical advantages and does not have big performance degradation. On the other hand, using a brute-forcing search to obtain the best BD signaling matrix is inefficient, and it is evident that a better solution can be provided.

Estimating the parameters of AmBC receivers needs calculations of the auto-correlation matrix of the received signal. It is deduced from this fact that the proposed receivers support any type of ambient signal with zero mean, which shows the generality of the receiver designs. Considering practical implementations of AmBC receivers, the dynamic range of ADC is a factor that limits AmBC receiver performance. The proposed implementation solutions mitigate the ADC dynamic range issue such that they improve the practicality of the proposed receiver designs.

An AmBC system under a wideband ambient signal is presented and the performance of multiple AmBC receivers built with COTS hardware is evaluated. The AmBC system parameters are decided based on the previous discussions on the practical implementation. For the wideband effect caused by uncontrollable COTS hardware, the processing method effectively mitigates the effect and yields a successful implementation. The measurement results show that the optimum receiver outperforms AmBC receivers in the literature.

The practical issues summarized in this chapter offer a comprehensive understanding of implementing AmBC systems. Such discussions and evaluations serve as an important component in actualizing the deployment of AmBC systems in practice.

5. Conclusion

The ultra-low-power, low-cost and spectrum-efficient AmBC is a key enabler enriching MTC use cases for the next generation of low-power wireless communications. New use-case possibilities are impeded by its poor BER performance in demodulating BD signals. This thesis focuses on improving the BER performance of the BD signal aiming for a wider deployment of AmBC technology (Publication I). The problem is tackled theoretically from the perspective of AmBC multi-antenna receiver design and BD signaling matrix design, and also practically by providing solutions regarding various implementational issues. Unlike available solutions that need to be tailored to specific system setups, the proposed designs attain higher practicality and generality. In particular, ambient signals are assumed with and without prior statistical information and the BD signal is assumed with general binary modulation. Two key factors for the poor BER performance including the strong DPI and unknown ambient signal are resolved by utilizing multi-antenna arrays. The results suggest that the multi-antenna AmBC receiver designs and BD designs improve AmBC system performance and outperform the state-of-the-art works.

The research of this thesis is based on the MAP criterion that minimizes the probability of error and yields optimal designs. It is shown that these designs are built upon the channels altered by BD transmissions. Compared to the direct path, the ambient signal propagating through the backscatter path experiences a phase offset caused by the excess path length, which is intricate to estimate and compensate. The phase-coherent operation can be accomplished by the coherent receiver (Publication III) applying an ML-assisted method. Taking the two paths as a composite channel rather than considering them individually brings various benefits for demodulating BD signal (Publication V). First, the optimum receiver in Publication V needs no DPI cancellation. Since the effect of the phase

offset is included in the composite channel, the optimum receiver implicitly obtains the phase offset when estimating the composite channel. Hence, second, it achieves the same performance as the coherent receiver, even though it does not require phase-coherent operations. Furthermore, the equivalence of the optimum receivers for a Gaussian-distributed ambient signal and for a deterministic-unknown ambient signal implies that the optimum receiver is generalized to much more practical scenarios. Therefore, the receiver designs improve the BER performance of the AmBC system and contribute significantly to the research field.

For improving the BER performance, one can place BDs at suitable locations, apply coding schemes at BDs, and/or use modulations with a large distance between states to increase the effective SNR of the BD signal. One can also apply the optimum BD signaling matrix on a multi-antenna BD (Publication VI) to steer the backscatter path signal in the direction with the strongest signal strength. In particular, it is shown from the BER performance that multi-antenna BDs make effective use of multiple RF sources, and the derived BD signaling matrices give a stable performance improvement compared to the widely adopted identity signaling matrix. Hence, the analyses offer insightful suggestions in regard to AmBC system deployments.

Practical implementations of the proposed designs are elaborated on. Results show that the proposed methods for estimating the beamformers and the BD signaling matrix on AmBC receivers when BDs send preambles are effective. Although estimating signaling matrices requires pilot information from ambient sources, the requirement can be circumvented by setting a predefined set of BD signaling matrices (Publication VI). Another identified practical restriction is the ADC dynamic range when a receiver is implemented in the digital domain. Receivers need the ADC to have a high dynamic range due to the extreme power difference between the backscatter signal and DPI. A hybrid implementation and a simplified receiver (Publication IV) that can be fully implemented in the analog domain are proposed as solutions. Even though the simplified receiver suffers from performance degradation, the hybrid implementation combats the dynamic range issue without a performance loss. The proposed multi-antenna receivers and receivers proposed in [19] are validated experimentally on low-cost hardware components. The BD and the receiver array are built in the research group with COTS and small form-factor hardware. The processing method proposed in Publication VII guarantees a successful

implementation of the multi-antenna receivers under a wideband ambient system, and the proposed optimum receiver outperforms others in the literature. Therefore, the discussions on implementations and the experiment greatly actualize the practical implementation of AmBC systems.

The designs and their practical implementation presented in this work are valid under certain assumptions. The scenarios when these assumptions are not satisfied provide some viable directions for future works. For instance, the objective function for the optimum BD signaling matrix is derived assuming that the ambient signal is known. A future work is to consider the case without knowing the ambient signal and derived the corresponding optimum BD signaling matrix. The BD is assumed to be synchronized with the AmBC receiver such that the BD frame is correctly detected at the AmBC receiver. In future work, the performance of using traditional synchronization sequences such as barker code or new synchronization schemes can be evaluated. The synchronization can be initialized by the AmBC receiver which sends an acknowledgment signal to allow the BD sends its information. Future work is also needed to tackle the ramifications caused by simultaneous transmissions from multiple BDs. One possible solution is to use BD identification or design proper BD scheduling to realize more realistic AmBC systems with multiple BDs. Furthermore, interference cancellation of BD signals for the target BD is necessary to improve the BER performance. One possibility is to apply orthogonal coding schemes on different BDs.

References

[1] P. Hu, P. Zhang, and D. Ganesan, "Laissez-faire: Fully asymmetric backscatter communication," in *Proceedings 2015 ACM Conference on Special Interest Group on Data Communication*, 2015, pp. 255–267.

[2] R. Zhao, P. Zhang, Y. Ma, and X. Zhang, "Ultra-wideband backscatter towards general passive iot localization," in *Proceedings of the 20th ACM Conference on Embedded Networked Sensor Systems*, 2022, 857–858.

[3] Z. Chi, X. Liu, W. Wang, Y. Yao, and T. Zhu, "Leveraging ambient LTE traffic for ubiquitous passive communication," in *Proceedings of the Annual Conference of the ACM Special Interest Group on Data Communication on the Applications, Technologies, Architectures, and Protocols for Computer Communication*, 2020, 172–185.

[4] P. Jonsson *et al.*, "Ericsson mobility report," Ericsson, Tech. Rep., November, 2022, p. 11.

[5] S. K. Sharma and X. Wang, "Toward massive machine type communications in ultra-dense cellular iot networks: Current issues and machine learning-assisted solutions," *IEEE Communications Surveys & Tutorials*, vol. 22, no. 1, pp. 426–471, 2020.

[6] N. H. Mahmood *et al.*, "Machine type communications: Key drivers and enablers towards the 6G era," *EURASIP Journal on Wireless Comunications and Networking*, vol. 2021, no. 134, 2021.

[7] 3GPP TR 38.848, "Technical specification group radio access network; study on ambient IoT (internet of things) in RAN," Tech. Rep., 2022.

[8] X. Lu, P. Wang, D. Niyato, D. I. Kim, and Z. Han, "Wireless networks with RF energy harvesting: A contemporary survey," *IEEE*

Communications Surveys & Tutorials, vol. 17, no. 2, pp. 757–789, 2015.

[9] D. M. Dobkin, *The RF in RFID: UHF RFID in practice*. Newnes: St Albans, UK, 2012.

[10] C. Boyer and S. Roy, "Backscatter communication and RFID: Coding, energy, and MIMO analysis," *IEEE Transactions on Communications*, vol. 62, no. 3, pp. 770–785, 2014.

[11] V. Liu, A. Parks, V. Talla, S. Gollakota, D. Wetherall, and J. R. Smith, "Ambient backscatter: Wireless communication out of thin air," in *Proceedings of the ACM SIGCOMM 2013 Conference on SIGCOMM*, 2013, pp. 39–50.

[12] D.-T. Phan-Huy, D. Barthel, P. Ratajczak, R. Fara, M. d. Renzo, and J. d. Rosny, "Ambient backscatter communications in mobile networks: Crowd-detectable zero-energy-devices," in *2021 IEEE International Conference on RFID Technology and Applications (RFID-TA)*, 2021, pp. 81–84.

[13] F. Jameel, R. Duan, Z. Chang, A. Liljemark, T. Ristaniemi, and R. Jäntti, "Applications of backscatter communications for healthcare networks," *IEEE Network*, vol. 33, no. 6, pp. 50–57, 2019.

[14] G. Vannucci, A. Bletsas, and D. Leigh, "A software-defined radio system for backscatter sensor networks," *IEEE Transactions on Wireless Communications*, vol. 7, no. 6, pp. 2170–2179, 2008.

[15] J. Griffin and G. Durgin, "Complete link budgets for backscatter-radio and RFID systems," *IEEE Antennas and Propagation Magazine*, vol. 51, no. 2, pp. 11–25, 2009.

[16] M. U. Sheikh, R. Duan, and R. Jäntti, "Validation of backscatter link budget simulations with measurements at 915 MHz and 2.4 GHz," in *2019 IEEE 89th Vehicular Technology Conference (VTC2019-Spring)*, 2019, pp. 1–5.

[17] C. He, S. Chen, H. Luan, X. Chen, and Z. J. Wang, "Monostatic mimo backscatter communications," *IEEE Journal on Selected Areas in Communications*, vol. 38, no. 8, pp. 1896–1909, 2020.

[18] X. Liu, Z. Chi, W. Wang, Y. Yao, and T. Zhu, "VMscatter: A versatile MIMO backscatter," in *17th USENIX Symposium on Networked Systems Design and Implementation (NSDI 20)*, 2020, pp. 895–909.

[19] H. Guo, Q. Zhang, S. Xiao, and Y. Liang, "Exploiting multiple antennas for cognitive ambient backscatter communication," *IEEE Internet Things Journal*, vol. 6, no. 1, pp. 765–775, 2019.

[20] J. Griffin and G. Durgin, "Gains for RF tags using multiple antennas," *IEEE Transactions on Antennas Propagation*, vol. 56, no. 2, pp. 563–570, 2008.

[21] W. Liu, S. Shen, D. H. K. Tsang, and R. Murch, "Enhancing ambient backscatter communication utilizing coherent and non-coherent space-time codes," *IEEE Transactions on Wireless Communications*, vol. 20, no. 10, pp. 6884–6897, 2021.

[22] S. M. Kay, *Fundamentals of statistical signal processing, Volume II: Detection Theory*. Upper Saddle River, NJ, USA: Prentice-Hall, Inc., 1993.

[23] Q. Tao, C. Zhong, X. Chen, H. Lin, and Z. Zhang, "Optimal detection for ambient backscatter communication systems with multi-antenna reader under complex gaussian illuminator," *IEEE Internet of Things Journal*, vol. 7, no. 12, pp. 11 371–11 383, 2020.

[24] M. Katanbaf, V. Jain, and J. R. Smith, "Relacks: Reliable backscatter communication in indoor environments," *Proceedings of the ACM on Interactive, Mobile, Wearable and Ubiquitous Technologies*, vol. 4, no. 2, pp. 1–24, 2020.

[25] W. Gong, L. Yuan, Q. Wang, and J. Zhao, "Multiprotocol backscatter for personal IoT sensors," in *Proceedings of the 16th International Conference on Emerging Networking EXperiments and Technologies*, 2020, 261–273.

[26] V. Iyer, V. Talla, B. Kellogg, S. Gollakota, and J. Smith, "Inter-technology backscatter: Towards internet connectivity for implanted devices," in *Proceedings of the 2016 ACM SIGCOMM Conference*, 2016, pp. 356–369.

[27] M. Lazaro, A. Lazaro, and R. Villarino, "Long-range lorawan backscatter based sensors for medical and wearable applications," in *2021 51st European Microwave Conference (EuMC)*, 2022, pp. 777–780.

[28] V. Talla, M. Hessar, B. Kellogg, A. Najafi, J. R. Smith, and S. Gollakota, "LoRa backscatter: Enabling the vision of ubiquitous connectivity," *Proceedings of the ACM on Interactive, Mobile, Wearable and Ubiquitous Technologies*, vol. 1, no. 3, pp. 1–24, 2017.

[29] D. Bharadia, K. Johsi, M. Kotaru, and S. Katti, "BackFi: High throughput WiFi backscatter," in *Proceedings of the 2015 ACM Conference on Special Interest Group on Data Communication*, 2015, pp. 283–296.

[30] H. Hwang, J. H. Lim, J. Yun, and B. J. Jeong, "Pattern-based decoding for Wi-Fi backscatter communication of passive sensors," *Sensors*, vol. 19, no. 5, 2019.

[31] A. Wang, V. Iyer, V. Talla, J. R. Smith, and S. Gollakota, "FM backscatter: Enabling connected cities and smart fabrics," in *Proceedings 14th USENIX Symposium on Networked Systems Design and Implementation (NSDI 17)*, 2017, pp. 243–258.

[32] K. Ruttik, X. Wang, J. Liao, R. Jäntti, and P.-H. Dinh-Thuy, "Ambient backscatter communications using LTE cell specific reference signals," in *2022 IEEE 12th International Conference on RFID Technology and Applications (RFID-TA)*, 2022, pp. 67–70.

[33] A. N. Parks, A. Liu, S. Gollakota, and J. R. Smith, "Turbocharging ambient backscatter communication," in *Proceedings ACM SIGCOMM*, 2014, pp. 619–630.

[34] M. L. Memon, N. Saxena, A. Roy, and D. R. Shin, "Backscatter communications: Inception of the battery-free era—a comprehensive survey," *Electronics*, vol. 8, no. 2, 2019.

[35] J. Kimionis, A. Georgiadis, S. N. Daskalakis, and M. M. Tentzeris, "A printed millimetre-wave modulator and antenna array for backscatter communications at gigabit data rates," *Nature Electronics*, vol. 4, pp. 439–446, 2021.

[36] P. V. Nikitin, S. Ramamurthy, R. Martinez, and K. V. S. Rao, "Passive tag-to-tag communication," in *2012 IEEE International Conference on RFID (RFID)*, 2012, pp. 177–184.

[37] A. Bletsas, P. N. Alevizos, and G. Vougioukas, "The art of signal processing in backscatter radio for μw (or less) internet of things: Intelligent signal processing and backscatter radio enabling batteryless connectivity," *IEEE Signal Processing Magazine*, vol. 35, no. 5, pp. 28–40, 2018.

[38] R. J. Vyas, B. B. Cook, Y. Kawahara, and M. M. Tentzeris, "E-WEHP: A batteryless embedded sensor-platform wirelessly powered

from ambient digital-TV signals," *IEEE Transactions on Microwave Theory and Techniques*, vol. 61, no. 6, pp. 2491–2505, 2013.

[39] G. Papotto, F. Carrara, A. Finocchiaro, and G. Palmisano, "A 90-nm cmos 5-Mbps crystal-less RF-powered transceiver for wireless sensor network nodes," *IEEE Journal of Solid-State Circuits*, vol. 49, pp. 335–346, 2014.

[40] F. Jameel, T. Ristaniemi, and B. M. Lee, "Simultaneous harvest-and-transmit ambient backscatter communications under rayleigh fading," *EURASIP Journal on Wireless Communications and Networking*, no. 166, 2019.

[41] D. T. Hoang, D. Niyato, P. Wang, D. I. Kim, and Z. Han, "Ambient backscatter: A new approach to improve network performance for RF-powered cognitive radio networks," *IEEE Transactions on Communications*, vol. 65, no. 9, pp. 3659–3674, 2017.

[42] R. Kishore, S. Gurugopinath, P. C. Sofotasios, S. Muhaidat, and N. Al-Dhahir, "Opportunistic ambient backscatter communication in RF-powered cognitive radio networks," *IEEE Transactions on Cognitive Communications and Networking*, vol. 5, no. 2, pp. 413–426, 2019.

[43] B. Kellogg, V. Talla, J. R. Smith, and S. Gollakota, "Passive Wi-Fi: Bringing low power to Wi-Fi transmissions," *GetMobile: Mobile Computing and Communications*, vol. 20, no. 3, 38–41, 2017.

[44] M. U. Sheikh, F. Jameel, H. Yiğitler, X. Wang, and R. Jäntti, "Monostatic backscatter communication in urban microcellular environment using cellular networks," in *2020 IEEE Wireless Communications and Networking Conference (WCNC)*, 2020, pp. 1–6.

[45] P. V. Nikitin and K. V. S. Rao, "Theory and measurement of backscattering from RFID tags," *IEEE Antennas and Propagation Magazine*, vol. 48, no. 6, pp. 212–218, 2006.

[46] D. Belo, R. Correia, Y. Ding, S. N. Daskalakis, G. Goussetis, A. Georgiadis, and N. B. Carvalho, "IQ impedance modulator front-end for low-power lora backscattering devices," *IEEE Transactions on Microwave Theory and Techniques*, vol. 67, no. 12, pp. 5307–5314, 2019.

[47] R. Hansen, "Relationships between antennas as scatterers and as radiators," *Proceedings of the IEEE*, vol. 77, no. 5, pp. 659–662, 1989.

[48] N. Van Huynh, D. T. Hoang, X. Lu, D. Niyato, P. Wang, and D. I. Kim, "Ambient backscatter communications: A contemporary survey," *IEEE Communications Surveys and Tutorials*, vol. 20, no. 4, pp. 2889–2922, 2018.

[49] C. Xu, L. Yang, and P. Zhang, "Practical backscatter communication systems for battery-free internet of things: A tutorial and survey of recent research," *IEEE Signal Processing Magazine*, vol. 35, no. 5, pp. 16–27, 2018.

[50] J. Kimionis, A. Bletsas, and J. N. Sahalos, "Increased range bistatic scatter radio," *IEEE Transactions on Communications*, vol. 62, no. 3, pp. 1091–1104, 2014.

[51] B. Kellogg, A. Parks, S. Gollakota, J. R. Smith, and D. Wetherall, "Wi-Fi backscatter: Internet connectivity for RF-powered devices," *ACM SIGCOMM Computer Communication Review*, vol. 44, no. 4, pp. 607–618, 2014.

[52] R. Duan, R. Jäntti, A. E. Mohamed, H. Zhu, and P. Miao, "Multi-antenna receiver for ambient backscatter communication systems," in *2018 IEEE 19th International Workshop on Signal Processing Advances in Wireless Communications (SPAWC)*, 2018.

[53] R. Duan, E. Menta, H. Yigitler, R. Jäntti, and Z. Han, "Hybrid beamformer design for high dynamic range ambient backscatter receivers," in *2019 IEEE Interational Conference on Communications Workshops (ICC Workshops)*, 2019, pp. 1–6.

[54] J. Qian, A. N. Parks, J. R. Smith, F. Gao, and S. Jin, "IoT communications with M-PSK modulated ambient backscatter: Algorithm, analysis, and implementation," *IEEE Internet of Things Journal*, vol. 6, no. 1, pp. 844–855, 2019.

[55] P. Zhang, M. Rostami, P. Hu, and D. Ganesan, "Enabling practical backscatter communication for on-body sensors," in *Proceedings of the 2016 ACM SIGCOMM Conference*, ACM, 2016, pp. 370–383.

[56] G. Vougioukas and A. Bletsas, "Switching frequency techniques for universal ambient backscatter networking," *IEEE Journal on Selected Areas in Communications*, vol. 37, no. 2, pp. 464–477, 2019.

[57] S. J. Thomas and M. S. Reynolds, "A 96 mbit/sec, 15.5 pj/bit 16-QAM modulator for UHF backscatter communication," in *2012 IEEE International Conference on RFID (RFID)*, 2012, pp. 185–190.

[58] S. N. Daskalakis, J. Kimionis, A. Collado, G. Goussetis, M. M. Tentzeris, and A. Georgiadis, "Ambient backscatterers using FM broadcasting for low cost and low power wireless applications," *IEEE Transactions on Microwave Theory and Techniques*, vol. 65, no. 12, pp. 5251–5262, 2017.

[59] Q. Tao, C. Zhong, K. Huang, X. Chen, and Z. Zhang, "Ambient backscatter communication systems with MFSK modulation," *IEEE Transactions on Wireless Communications*, vol. 18, no. 5, pp. 2553–2564, 2019.

[60] R. Duan, R. Jäntti, H. Yiğitler, and K. Ruttik, "On the achievable rate of bistatic modulated rescatter systems," *IEEE Transactions on Vehicular Technology*, vol. 66, no. 10, pp. 9609–9613, 2017.

[61] D. Darsena, G. Gelli, and F. Verde, "Modeling and performance analysis of wireless networks with ambient backscatter devices," *IEEE Transactions on Communications*, vol. 65, no. 4, pp. 1797–1814, 2017.

[62] E. Basar, M. Di Renzo, J. De Rosny, M. Debbah, M.-S. Alouini, and R. Zhang, "Wireless communications through reconfigurable intelligent surfaces," *IEEE Access*, vol. 7, pp. 116 753–116 773, 2019.

[63] C. A. Balanis, *Antenna theory: analysis and design*, 3rd. Wiley-Interscience, 2005.

[64] A. Bletsas, A. G. Dimitriou, and J. N. Sahalos, "Improving backscatter radio tag efficiency," *IEEE Transactions on Microwave Theory and Techniques*, vol. 58, no. 6, pp. 1502–1509, 2010.

[65] C. Chen, G. Wang, H. Guan, Y. Liang, and C. Tellambura, "Transceiver design and signal detection in backscatter communication systems with multiple-antenna tags," *IEEE Transactions on Wireless Communications*, vol. 19, no. 5, pp. 3273–3288, 2020.

[66] D. Chizhik, G. Foschini, M. Gans, and R. Valenzuela, "Keyholes, correlations, and capacities of multielement transmit and receive antennas," *IEEE Transactions on Wireless Communications*, vol. 1, no. 2, pp. 361–368, 2002.

[67] R. Biswas, M. U. Sheikh, H. Yiğitler, J. Lempiäinen, and R. Jäntti, "Direct path interference suppression requirements for bistatic backscatter communication system," in *2021 IEEE 93rd Vehicular Technology Conference (VTC2021-Spring)*, 2021, pp. 1–5.

[68] T. L. Nguyen, Y. Shin, J. Y. Kim, and D. I. Kim, "Signal detection for ambient backscatter communication with OFDM carriers," *Sensors*, vol. 19, no. 3, 2019.

[69] D. Darsena, "Noncoherent detection for ambient backscatter communications over OFDM signals," *IEEE Access*, vol. 7, pp. 159 415–159 425, 2019.

[70] G. Wang, F. Gao, R. Fan, and C. Tellambura, "Ambient backscatter communication systems: Detection and performance analysis," *IEEE Transactions on Communications*, vol. 64, no. 11, pp. 4836–4846, 2016.

[71] J. Qian, F. Gao, G. Wang, S. Jin, and H. Zhu, "Noncoherent detections for ambient backscatter system," *IEEE Transaction on Wireless Communications*, vol. 16, no. 3, pp. 1412–1422, 2017.

[72] J. K. Devineni and H. S. Dhillon, "Non-coherent detection and bit error rate for an ambient backscatter link in time-selective fading," *IEEE Transactions on Communications*, vol. 69, no. 1, pp. 602–618, 2021.

[73] G. Yang, Y.-C. Liang, R. Zhang, and Y. Pei, "Modulation in the air: Backscatter communication over ambient OFDM carrier," *IEEE Transactions on Communications*, vol. 66, no. 3, pp. 1219–1233, 2018.

[74] J. Lietzén, A. Liljemark, R. Duan, R. Jäntti, and V. Viikari, "Polarization conversion-based ambient backscatter system," *IEEE Access*, vol. 8, pp. 216 793–216 804, 2020.

[75] R. Fara, D. T. Phan-Huy, A. Ourir, Y. Kokar, J. C. Prévotet, M. Hélard, M. Di Renzo, and J. De Rosny, "Polarization-based reconfigurable tags for robust ambient backscatter communications," *IEEE Open Journal of the Communications Society*, vol. 1, pp. 1140–1152, 2020.

[76] M. A. ElMossallamy, M. Pan, R. Jäntti, K. G. Seddik, G. Y. Li, and Z. Han, "Noncoherent backscatter communications over ambient

OFDM signals," *IEEE Transactions on Communications*, vol. 67, no. 5, pp. 3597–3611, 2019.

[77] Q. Tao, C. Zhong, X. Chen, H. Lin, and Z. Zhang, "Maximum-eigenvalue detector for multiple antenna ambient backscatter communication systems," *IEEE Transactions on Vehicular Technology*, vol. 68, no. 12, pp. 12 411–12 415, 2019.

[78] G. Yang, Q. Zhang, and Y. Liang, "Cooperative ambient backscatter communications for green Internet-of-Things," *IEEE Internet of Things Journal*, vol. 5, no. 2, pp. 1116–1130, 2018.

[79] C. H. Kang, W. S. Lee, Y. H. You, and H. K. Song, "Signal detection scheme in ambient backscatter system with multiple antennas," *IEEE Access*, vol. 5, pp. 14 543–14 547, 2017.

[80] T. Kim and W. Lee, "Anyscatter: Eliminating technology dependency in ambient backscatter systems," in *IEEE INFOCOM 2020 - IEEE Conference on Computer Communications*, 2020, pp. 287–296.

[81] J. Proakis and M. Salehi, *Digital communications*, 5th. New York: McGraw-Hill, 2008.

[82] Z. Ma, T. Zeng, G. Wang, and F. Gao, "Signal detection for ambient backscatter system with multiple receiving antennas," in *IEEE 14th Canadian Workshop on Information Theory (CWIT)*, 2015, pp. 50–53.

[83] Q. Zhang, H. Gao, Y. Liang, and X. Yuan, "Constellation learning lased signal detection for ambient backscatter communication systems," *IEEE Journal on Selected Areas in Communications*, vol. 37, no. 2, pp. 452–463, 2019.

[84] A. H. Raghavendra, A. K. Kowshik, S. Gurugopinath, S. Muhaidat, and C. Tellambura, "Generalized space shift keying for ambient backscatter communication," *IEEE Transactions on Communications*, vol. 70, no. 8, pp. 5018–5029, 2022.

[85] G. Yue, L. Ping, and X. Wang, "Generalized low-density parity-check codes based on Hadamard constraints," *IEEE Transactions on Information Theory*, vol. 53, no. 3, pp. 1058–1079, 2007.

[86] P. N. Alevizos, A. Bletsas, and G. N. Karystinos, "Noncoherent short packet detection and decoding for scatter radio sensor networking," *IEEE Transactions on Communications*, vol. 65, no. 5, pp. 2128–2140, 2017.

[87] P. N. Alevizos, N. Fasarakis-Hilliard, K. Tountas, N. Agadakos, N. Kargas, and A. Bletsas, "Channel coding for increased range bistatic backscatter radio: Experimental results," in *2014 IEEE RFID Technology and Applications Conference (RFID-TA)*, 2014, pp. 38–43.

[88] N. Fasarakis-Hilliard, P. N. Alevizos, and A. Bletsas, "Coherent detection and channel coding for bistatic scatter radio sensor networking," *IEEE Transactions on Communications*, vol. 63, no. 5, pp. 1798–1810, 2015.

[89] J. M. Wozencraft and I. M. Jacobs, *Principles of communication engineering*. New York: Wiley, 1965.

[90] R. Zhao, F. Zhu, Y. Feng, S. Peng, X. Tian, H. Yu, and X. Wang, "OFDMA-enabled Wi-Fi backscatter," in *MobiCom 19: The 25th Annual Interational Conference on Mobile Computing and Networking*, 2019.

[91] C. M. Bishop, *Pattern recognition and machine learning (Information science and statistics)*. Berlin, Heidelberg: Springer-Verlag, 2006.

[92] S. Kotz, T. Kozubowski, and K. Podgorski, *The Laplace distribution and generalizations: A revisit with applications to communications, economics, engineering, and finance* (Progress in Mathematics). Birkhäuser Boston, 2001.

[93] R. G. Gallager, *Principles of digital communication*. Cambridge University Press, 2008.

[94] H. W. Sorenson, *Parameter estimation: principles and problems*. M. Dekker, 1980, vol. 9.

[95] C. R. Rao, *Linear statistical inference and its applications*, 2nd. Wiley, 2008.

[96] D. Tse and P. Viswanath, *Fundamentals of wireless communication*, USA, 2005.

[97] S. Provost and E. Rudiuk, "The exact distribution of indefinite quadratic forms in noncentral normal vectors," *Annals of the Institute of Statistical Mathematics*, vol. 48, no. 2, pp. 381–394, 1996.

[98] N. Johnson, S. Kotz, and N. Balakrishnan, *Continuous univariate distributions*, 2nd. Wiley & Sons, 1995.

[99] M. S. Paolella, *Intermediate probability: A computational approach*. Wiley & Sons, 2007.

[100] R. Lugannani and S. Rice, "Saddle point approximation for the distribution of the sum of independent random variables," *Advances in Applied Probability*, vol. 12, no. 2, 475–490, 1980.

[101] T. Y. Al-Naffouri, M. Moinuddin, N. Ajeeb, B. Hassibi, and A. L. Moustakas, "On the distribution of indefinite quadratic forms in Gaussian random variables," *IEEE Transactions on Communications*, vol. 64, no. 1, pp. 153–165, 2016.

[102] J. K. Devineni and H. S. Dhillon, "Manchester encoding for noncoherent detection of ambient backscatter in time-selective fading," *IEEE Transactions on Vehicular Technology*, vol. 70, no. 5, pp. 5109–5114, 2021.

[103] P. Zhang, D. Bharadia, K. Joshi, and S. Katti, "Hitchhike: Practical backscatter using commodity WiFi," in *Proceedings of the 14th ACM Conference on Embedded Network Sensor Systems CD-ROM*, 2016, 259–271.

[104] Y. Peng, L. Shangguan, Y. Hu, Y. Qian, X. Lin, X. Chen, D. Fang, and K. Jamieson, "PLoRa: A passive long-range data network from ambient LoRa transmissions," in *Proceedings of the 2018 Conference of the ACM Special Interest Group on Data Communication*, 2018, pp. 147–160.

[105] G. H. Golub and C. F. Van Loan, *Matrix computations*, 4th. Johns Hopkins University Press Baltimore, 2013.

[106] R. Zhang, T. J. Lim, Y. Liang, and Y. Zeng, "Multi-antenna based spectrum sensing for cognitive radios: A GLRT approach," *IEEE Transactions on Communications*, vol. 58, no. 1, pp. 84–88, 2010.

[107] S. Yang, W. Lyu, D. Wang, and Z. Zhang, "Separate channel estimation with hybrid RIS-aided multi-user communications," *IEEE Transactions on Vehicular Technology*, vol. 72, no. 1, pp. 1318–1324, 2023.

[108] T. A. Siddiqui, J. Holopainen, and V. Viikari, "Beam-steerable transponder based on antenna array and phased modulators," *IEEE Antennas Wireless Propagation Letters*, vol. 20, no. 3, pp. 356–360, 2021.

[109] B. Wang, F. Gao, S. Jin, H. Lin, G. Y. Li, S. Sun, and T. S. Rappaport, "Spatial-wideband effect in massive MIMO with application in mmWave systems," *IEEE Communications Magazine*, vol. 56, no. 12, pp. 134–141, 2018.

Aalto-DT 117/2023

ISBN 978-952-64-1365-5 (printed)
ISBN 978-952-64-1366-2 (pdf)
ISSN 1799-4934 (printed)
ISSN 1799-4942 (pdf)

Aalto University
School of Electrical Engineering
Department of Information and Communications Engineering
www.aalto.fi

BUSINESS + ECONOMY

ART + DESIGN + ARCHITECTURE

SCIENCE + TECHNOLOGY

CROSSOVER

DOCTORAL THESES